# Bovine Serum Amine Oxidase and polyamine analogues: chemical synthesis and biological evaluation integrated with molecular docking and 3-D QSAR studies

| | |
|---|---|
| Journal: | *Journal of Chemical Information and Modeling* |
| Manuscript ID | ci-2022-00559e.R2 |
| Manuscript Type: | Article |
| Date Submitted by the Author: | n/a |
| Complete List of Authors: | Ragno, Rino; "Sapienza" University of Rome , Department of Drug Chemistry and Technology<br>Minarini, Anna; Universita degli Studi di Bologna, Pharmaceuticl Sciences<br>Proia, Eleonora; University of Rome La Sapienza, Department of Drug Chemistry and Technology<br>Antonini, Lorenzo; University of Rome La Sapienza, Department of chrmistry and technology of drug<br>Milelli, Andrea; Alma Mater Studiorum, University of Bologna, Department for Life Quality Studies<br>Tumiatti, Vincenzo; Universita degli Studi di Bologna, Department of Pharmaceutical Sciences<br>Fiore, Marco; IBCM-CNR,<br>Fino, Pasquale; University of Rome La Sapienza, 5UOC of Dermatology, Policlinico Umberto I Hospital<br>Rutigliano, Lavinia; University of Rome La Sapienza, Department of Sensory Organs<br>Fioravanti, Rossella; Università "La Sapienza" di Roma, Chimica e Tecnologie del Farmaco<br>Tahara, Tomoaki ; University of Rome La Sapienza, ìDepartment of Sensory Organs<br>Pacella, Elena; University of Rome La Sapienza<br>Greco, Antonio; University of Rome La Sapienza, Department of Sensory Organs<br>Canettieri, Gianluca; Sapienza University of Rome,<br>Di Paolo, Maria Luisa; Univ. of Padova, Chimica Biologica<br>Agostinelli, Enzo; Sapienza University, Department of Sensory Organs |
| | |

Journal of Chemical Information and Modeling

# New BSAO Substrates

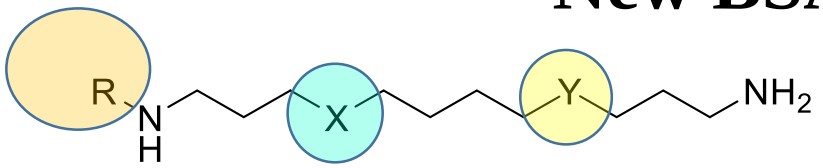


| # | R | X | Y | Km (μM) | $k_{cat}/K_m$ ($\mu M^{-1}\ s^{-1}$) |
|---|---|---|---|---|---|
| 10 | 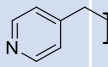 | N | N | 7.2 | 0.109 |
| 13 | 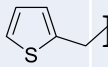 | N | N | 6.0 | 0.098 |
| 21 | 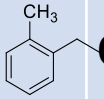 | O | O | 3.8 | 0.124 |

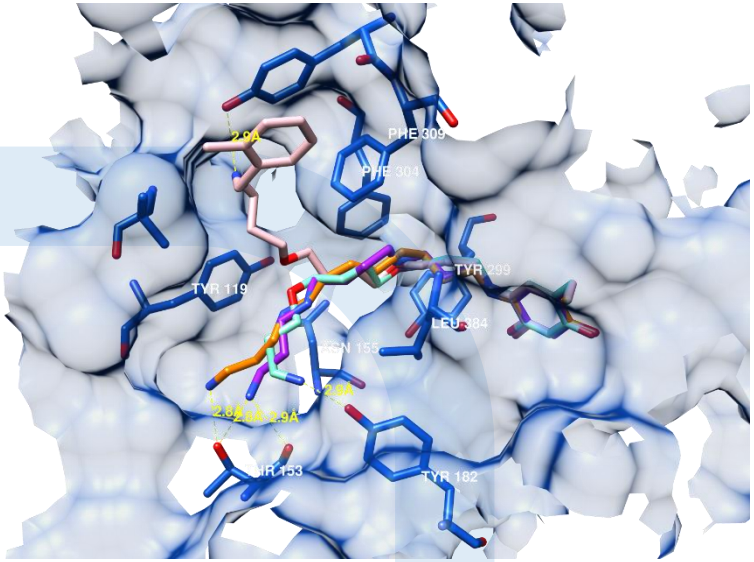


## Molecular Docking

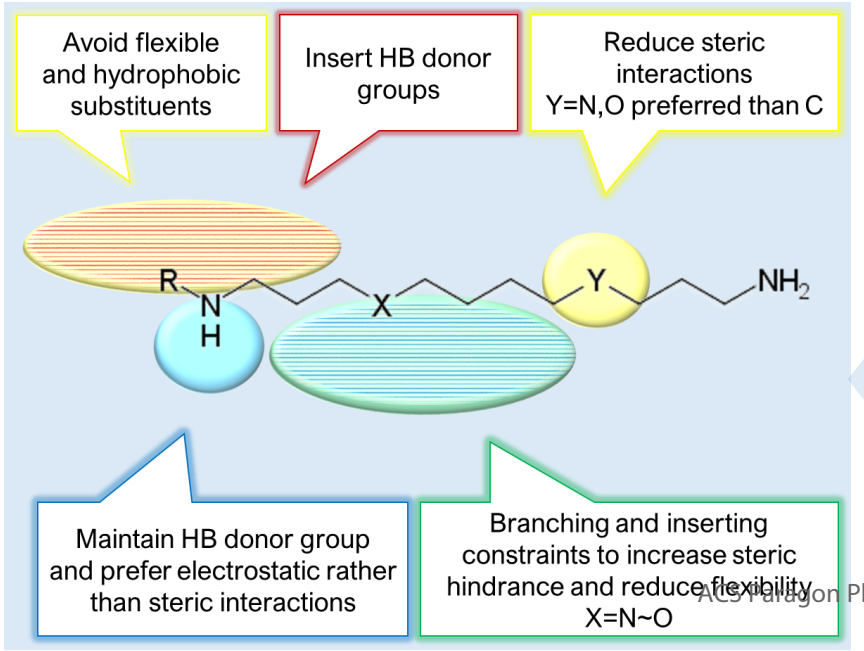


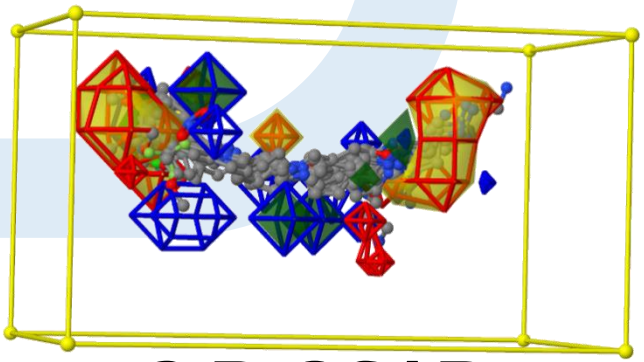

## 3-D QSAR

# Bovine Serum Amine Oxidase and polyamine analogues: chemical synthesis and biological evaluation integrated with molecular docking and 3-D QSAR studies

Rino Ragno,[1,‡] Anna Minarini,[2,‡] Eleonora Proia,[1] Antonini Lorenzo,[1] Andrea Milelli,[3] Vincenzo Tumiatti,[3] Marco Fiore,[4] Pasquale Fino,[5] Lavinia Rutigliano,[6] Rossella Fioravanti,[7] Tomoaki Tahara,[6] Elena Pacella,[6] Antonio Greco,[6] Gianluca Canettieri,[8,9] Maria Luisa Di Paolo[10,*] and Enzo Agostinelli[6,11,*]

[1] Rome Center for Molecular Design, Department of Drug Chemistry and Technology, Sapienza Università di Roma, P. le A. Moro 5, 00185 Roma, Italy, rino.ragno@uniroma1.it (R.R.); lorenzo.antonini@uniroma1.it (L.A.); eleonora.proia@uniroma1.it (E.P.)

[2] Department of Pharmacy and Biotechnology, Alma Mater Studiorum-University of Bologna, Via Belmeloro 6, 40126, Bologna, Italy, anna.minarini@unibo.it (A.M.)

[3] Department for Life Quality Studies, Alma Mater Studiorum-University of Bologna, Corso d'Augusto, 237, 47921, Rimini, Italy, andrea.milelli3@unibo.it (A.MI.); vincenzo.tumiatti@unibo.it (V.T)

[4]Department Institute of Biochemistry and Cell Biology, IBBC-CNR, Via E. Ramarini, 32 – 00015 Monterotondo Scalo Rome, Italy; marco.fiore@cnr.it (M.F.)

[5]UOC of Dermatology, Policlinico Umberto I Hospital, Sapienza Medical School of Rome, Viale del Policlinico 155, I-00161 Rome, Italy; pasquale.fino@gmail.com (P.F.)

[6]Department of Sensory Organs, Sapienza University of Rome, Policlinico Umberto I, Viale del Policlinico155, I-00161 Rome, Italy; tahara.1943656@studenti.uniroma1.it (T.T.); lavinia.rutigliano@uniroma1.it (L.R.); elena.pacella@uniroma1.it (EP); antonio.greco@uniroma1.it (A.G.); enzo.agostinelli@uniroma1.it (E.A.)

[7]Department of Drug Chemistry and Technology, Sapienza Università di Roma, P. le A. Moro 5, 00185 Roma, Italy, rossella.fioravanti@uniroma1.it (R.F.);

[8]Department of Molecular Medicine, Sapienza University of Rome, Viale Regina Elena 291, 00161 Rome, Italy;

[9]Istituto Pasteur, Fondazione Cenci-Bolognetti, Sapienza University of Rome, Viale Regina Elena 291, 00161 Rome, Italy gianluca.canettieri@uniroma1.it (G.C.)

[10]Department of Molecular Medicine, University Padua, Via G. Colombo 3, 35131 Padova, Italy; marialuisa.dipaolo@unipd.it; (M.L.D.P.)

[11]International Polyamines Foundation 'ETS-ONLUS' Via del Forte Tiburtino 98, I-00159 Rome, Italy; polyfoundation2017@gmail.com.

* Corresponding authors: enzo.agostinelli@uniroma1.it and marialuisa.dipaolo@unipd.it

‡ these authors contributed equally to this work

This work is a tribute to Giampiero Tempera Ph.D.

**Abbreviations**: BSAO: bovine serum amine oxidase; PA: polyamine; SB: structure-based; LB ligand-based; 3-D QSAR: three-dimensional quantitative structure-activity relationships; ComBinE: comparative binding energy; MDock: molecular docking; CMDock: covalent molecular docking; RMDock: reversible molecular docking; Spm: spermine.

**Abstract**

Natural polyamines (PAs) are key players in cellular homeostasis by regulating cell growth and proliferation. Several observations highlight that polyamines (PAs) are also implicated in pathways regulating cell death. Indeed, the PAs accumulation cytotoxic effect, maximized with the use of Bovine Serum Amine Oxidase (BSAO) enzyme, represents a valuable strategy against tumor progression. In the present study, along with the design, synthesis and biological evaluation of a series of new spermine (Spm) analogs (**1-23)**, a mixed Structure-Based (SB) and Ligand-Based (LB) protocol was applied. Binding modes of BSAO-PA modeled complexes led to clarify electrostatic and steric features likely affecting the BSAO-PA biochemical kinetics. LB and SB Three-Dimensional Quantitative Structure-Activity Relationship (Py-CoMFA and Py-ComBinE) models were developed by means of the 3d-qsar.com portal and their analysis represent a strong basis for future design and synthesis of PAs BSAO substrates for potential application in oxidative stress-induced chemotherapy.

## Introduction

The natural polyamines (PAs) putrescine (Put), spermidine (Spd) and spermine (Spm), are ubiquitous polycationic molecules present in all organism cells, where they support a wide variety of cellular functions.[1] Due to their polycationic structures, PAs are able to interact with various biological macromolecules, such as nucleic acids, phospholipids and proteins (receptors, ionic channels and enzymes), thus modulating various metabolic and signaling pathways. Indeed, PAs are involved in cellular homeostasis, cell growth, proliferation, and cell death.[1] The dysregulation of PA metabolism is associated with various pathological conditions. In particular, the PA biosynthetic pathway is very active during cancer cell growth, and PA content is increased in tumor cells and tissues, such as breast, colon, skin and prostate cancers.[2, 3] Given the role of natural polyamines in cancer, efforts have been made in search for strategies that target the PA metabolism, which might be useful for tumor treatment.[4, 5] In this context, the main investigated strategies have been pointed to reduce intracellular PA concentration by inhibition of their synthesis or transport across cell membranes, as well as through the use of analogues that interfere with PA metabolism. More recently, the strategy of exploiting PA-degrading enzymes to induce cancer cells death has been applied.[5, 6] Indeed, the oxidative deamination of PAs catalyzed by some amine oxidases causes an over-production of aldehydes and hydrogen peroxide, which are cytotoxic and can damage cancer cells causing apoptosis/necrosis, and ultimately cell death.[7-11] The induction of oxidative stress by increasing ROS has recently received great attention in anticancer therapies and the effect of various anticancer drugs is based on the principle of oxidative stress-induced chemotherapy,[12] for example, 2-methoxyestradiol induces mitochondrial production of hydrogen peroxide and subsequently activates c-Jun N-terminal kinase (JNK), resulting in apoptosis initiation.[13]

Therefore, the induction of Spm oxidase by PA analogues[13, 14] or the simultaneous delivery of bovine serum amine oxidase (BSAO) with Spm to produce polyamine metabolites are currently explored as a promising strategy in tumor therapy.[15-19]

In particular, the possibility of assembling both BSAO and/or PA analogues in nanoparticles to target cancer cells is recently been explored and seems very promising in this field.[15, 17, 20] BSAO is a copper and semicarbazide-sensitive-amine oxidase, whose crystal 3D-structure has been resolved, either alone (PDB entry code 1TU5) or complexed with clonidine[21, 22] (PDB entry code

2PNC). Currently, no BSAO crystal structure complexed with a PA derivative is yet available. The structural studies on BSAO together with the functional studies performed with different substrates, gave information about the most important molecular properties (aliphatic chain length, charge distribution, steric hindrance) for an efficient BSAO substrate.[23-26] In particular, under physiological conditions, the electrostatic interaction between the positively charged polyamine skeleton and the active site of the enzyme play a crucial role, together with the flexibility of the BSAO secondary structure, which enable the enzyme to accommodate even sterically hindered substrate(s).[21, 23] Further studies are needed to perform structural optimization of BSAO substrate(s) useful for this specific application in anticancer therapies: substrate(s) for which BSAO should demonstrate high affinity and catalytic efficiency; they should be easily delivered into cells and soluble under physiological conditions. Molecular docking (MDock),[27] ligand-based (LB) and structure-based (SB) three-dimensional quantitative structure-activity relationships[28] (3-D QSAR) and comparative molecular binding analysis[29-31] (COMBINE) are well- recognized tools to develop quantitative models with the aim to investigate on both the binding mode and the main chemical features taking part to the ligand-macromolecule interaction.

Herein a series of new Spm analogues (**1-23**, Figure 1 and Table 1), characterized by different aryl methyl substituents on one primary amino group of Spm, was designed, synthesized and used as BSAO active site probes through extensive biological kinetic analysis. The experimental data were then integrated with a molecular modeling protocol including reversible and covalent MDock simulations and structure-based (SB) and ligand-based (LB) quantitative methods to shed light on the main features guiding the BSAO/PA interactions for future drug design of new and more effective PA analogues.

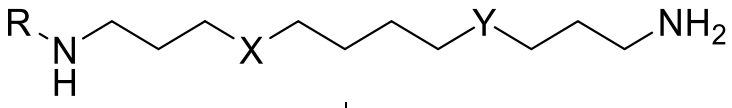


| | R | X | Y | | R | X | Y |
|---|---|---|---|---|---|---|---|
| **1** | 4-$CH_3$-$C_6H_4CH_2$ | N | N | **13** | 2-$C_4H_3SCH_2$ | N | N |
| **2** | 4-$CH_3O$-$C_6H_4CH_2$ | N | N | **14** | 2-$CF_3$-$C_6H_4CH_2$ | N | N |
| **3** | $C_6H_5CH_2$ | N | N | **15** | 2-F-$C_6H_4CH_2$ | N | N |
| **4** | 2-$CH_3$-$C_6H_4CH_2$ | N | N | **16** | 3-$CH_3O$-4-OH-$C_6H_3CH_2$ | N | N |
| **5** | 2-$NO_2$-$C_6H_4CH_2$ | N | N | **17** | 2-$CH_3O$-$C_6H_4CH_2$ | N | N |
| **6** | 2-Cl-$C_6H_4CH_2$ | N | N | **18** | H | N | C |

| | | | | | | | |
|---|---|---|---|---|---|---|---|
| **7** | 2,3,4-$CH_3O$-$C_6H_4CH_2$ | N | N | **19** | 2-$CH_3$-$C_6H_4CH_2$ | N | C |
| **8** | 3,4,5-$CH_3O$-$C_6H_4CH_2$ | N | N | **20** | 2-$C_4H_3SCH_2$ | N | C |
| **9** | 2-$C_5H_5N$ | N | N | **21** | 2-$CH_3$-$C_6H_4CH_2$ | O | O |
| **10** | 4-$C_5H_5N$ | N | N | **22** | 2-$C_4H_3SCH_2$ | O | O |
| **11** | 3-$C_5H_5N$ | N | N | **23** | H | O | O |
| **12** | 2-$C_{10}H_7CH_2$ | N | N | **Spm** | H | N | N |

**Figure 1.** General structure of the newly synthesized Spm analogues **1-23** as BSAO substrates

## Results and discussion

### Structural design of PA analogues

The structure modifications applied on the Spm scaffold, concerned the insertion of unsubstituted and substituted (hetero)aromatic rings on one of the primary amine functions, and the replacement of one or both the inner secondary amine groups in order to explore the activity towards BSAO. In particular, compounds **1-8** and **14-17** as direct Spm derivatives are characterized by a benzyl ring, carrying substituents with different steric or electronic properties. Spm was also substituted with a larger aromatic ring, such as naphthalene (**12**), and heteroaromatic rings, such as pyridine (**9-11**) and thiophene (**13**). To evaluate the importance of a polycationic chain in favor of BSAO activity, triamine derivatives **18-20** and diamines **21** and **22,** the commercially available Spm dioxa analogues (**23**) and Spm were also included in the study. In particular, one of the Spm and compounds **4** and **13** inner nitrogen atoms was isosterically replaced with a methylene group, affording compounds **18, 19** and **20**, respectively, while the replacement of both inner nitrogen atoms of compounds **4** and **13** with oxygen atoms led to diamino-ether derivatives **21** and **22**, respectively.

### Chemistry

The synthesis of the PA analogues are reported in Schemes 1 and 2. Tetraamines **3, 4**,[32] **17**,[33] **16**,[34] **12**, **13**, **20** and **22**[35] were synthesized as previously reported. Tetraamines **1**, **2**, **5-11**, **14** and **15** were synthesized as depicted in Scheme 1: the appropriate aldehydes were reacted with tri-Boc-spermine[36] to afford the corresponding Schiff bases which were reduced in situ to give compounds **24-34**; acidic deprotection of such compounds led to the corresponding tetraamines **1**, **2**, **5-11**, **14** and **15** as tetrahydrochloride salts.

Preparation of **19** and **21** was performed as shown in Scheme 2. Briefly, 2-methylbenzaldehyde was let to react with the proper mono-Boc-protected diamines **35** and **36**[35] to result the corresponding Schiff bases which were reduced in situ to give compounds **37** and **38**, respectively; acidic deprotection of such compounds led to the corresponding target compounds **19** and **21** as dihydrochloride salts, respectively.

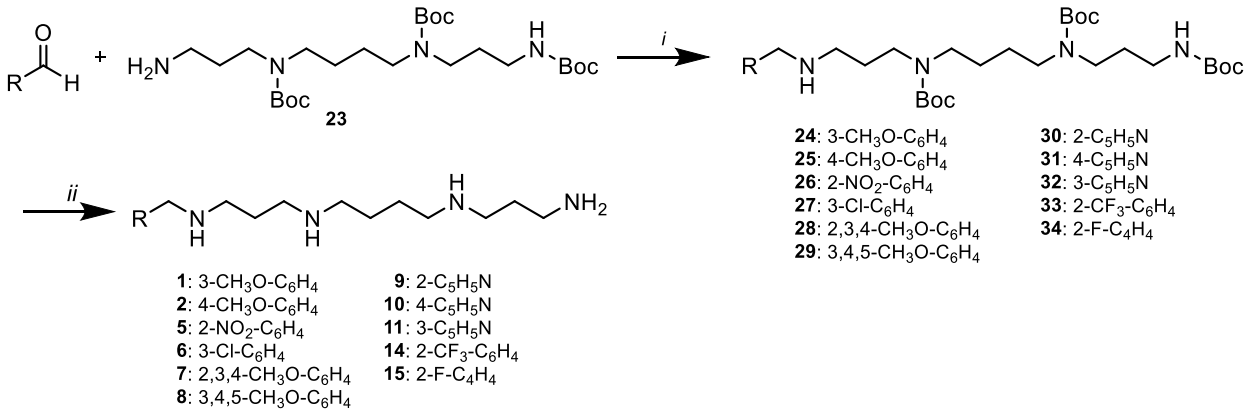


**Scheme 1.** (*i*) (a) toluene/Δ/3 h, (b) $NaBH_4$/EtOH/rt/4 h, (*ii*) HCl 3M/rt/overnight; Boc = $(CH_3)_3COCO$-

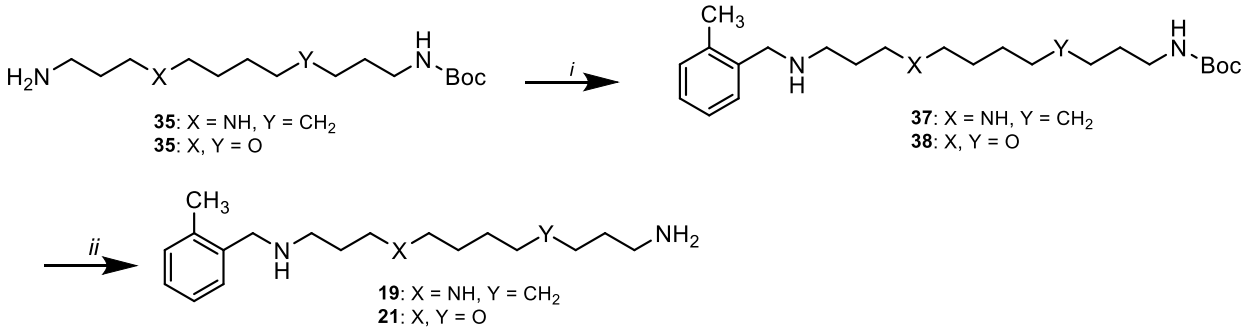


**Scheme 2.** (*i*) (a) 2-$CH_3$-$C_6H_4CHO$, toluene, reflux, 3 h, (b) $NaBH_4$, EtOH, rt, 4h; (*ii*) HCl 3M, rt, overnight quantitative yields; Boc = $(CH_3)_3COCO$-

**Biological assay. Kinetic parameters of BSAO for the various polyamine analogues**

The PA derivatives **1-23** were evaluated through biological assays aimed to determine their kinetic parameters. The $K_M$ values showed that the affinity of BSAO for the various analogs spanned in the range 2-100 μM. Even if BSAO showed the best affinity (lowest $K_M$ values), for either the

physiological Spm or the dioxadiamine Dioxa (**23**), some analogues were also found to be adequate BSAO substrates. In particular, **4**, **10**, **12** and **13**, among the Spm derivatives, and **20** (triamines) and **21**, **22** (diamines) showed $K_M$ values in the single digit micromolar range. Low affinity, that is high $K_M$ value, was obtained for **3**, **6**, **7**, **15**, and **19**, being the last one with the lowest affinity among all the tested compounds ($K_M$ = 97 μM). This strong effect on $K_M$ values depending on the substituents (R) on the primary amine of Spm skeleton ("N-$C_{(3)}$-N-$C_{(4)}$-N-$C_{(3)}$-N"), likely indicates the important role of this moiety in substrate docking /anchoring into BSAO active site. The catalytic constant ($k_{cat}$) values spanned in the range 0.15-1.5 $s^{-1}$, that is in a narrower range than that of $K_M$. In addition to Spm, ($k_{cat}$ =1.5 $s^{-1}$), the highest $k_{cat}$ values (1.29-0.91$s^{-}$1) were found for **8**, **9**, **11** and **23**. Most of the other $k_{cat}$ values spanned in the range 0.46-0.80 $s^{-1}$; $k_{cat}$ values lower than 0.45 were found only for **4**, **12**, **18** and **19**, being this last one the less effective substrate ($k_{cat}$ =0.04 $s^{-1}$). These data suggest that the different type of moiety bonded at the SPM tail could affect the chemical step of the oxidative deamination of the substrate ($H_2O_2$ and aldehyde production and release).

The BSAO catalytic efficiency values ($k_{cat}/K_M$) for these compounds, a kinetic parameter that controls the reaction rate under the non-saturating concentration of substrate ([S]<<$K_M$), were found to be lower than that for the physiological Spm substrate, with the exception of **23**, for which a catalytic efficiency 1,2 times that for SPM was found. For the other compounds, if compared to Spm, the resulting relative catalytic efficiency values, ($k_{cat}/K_M$)/($k_{cat}/K_{M\_Spm}$), were higher than 0.2 ($kc/K_M$> 0.1 $\mu M^{-1}$ $s^{-1}$) for **8**, **10**, **13** and **21** only. The other relative catalytic efficiency values were in the medium range 0.2-0.1 for **9**, **11**, **12, 20** and **22** ($k_{cat}/K_M$ values in the range 0.1-0.05 $\mu M^{-1}s^{-1}$), and lower of more than one order of magnitude for the other compounds (relative catalytic efficiency< 0.1), being **19** the compound with the lowest catalytic efficiency ($k_{cat}/K_M$ = 0.0004 $\mu M^{-1}s^{-1}$).

The lack of one of the secondary amine groups in the PA skeleton as in triamine **18**, (N-$C_{(3)}$-N-$C_{(4)}$-C-$C_{(3)}$-N *vs* Spm) led to a decrease in the $k_{cat}$ value (0.31 *vs* 1.5 $s^{-1}$), even more relevant in compounds **4** and **19**, bearing a toluene ring with an associated lowest affinity (the highest $K_M$ value), $k_{cat}$ and $k_{cat}/K_M$. Differently, the substitution of both of the secondary amine groups with oxygen atoms in the Spm skeleton as in **23**, determined a decrease in $k_{cat}$ value (0.9 *vs* 1.5 $s^{-1}$ of Spm) and improved the affinity and catalytic efficiency respect to Spm. Also, in this case, the

addition of a toluene ring on the tail (compound **21**) induced a decrease in the affinity and catalytic constant compared to **23**, even if not so strong of that observed as in the case of the triamine (**18** *vs* **19**).

Among the tested analogues, the non-physiological substrates with the best profile in terms of low $K_M$ and high $k_{cat}$ and $k_{cat}/K_M$ values among the tested analogues were the tetramines **8** and **10** and the diamine **23** , bearing a trimethoxy benzyl and a pyridinyl moiety, suggesting the importance of both the role of the Spm skeleton and the substituents in the recognition of the active site of BSAO and therefore on the associated catalytic process. Additionally, **13** and **21**, endowed with high affinity ($K_M$) and significant catalytic efficiency ($k_{cat}/K_M$), even though with an average $k_{cat}$ value, can be considered as interesting BSAO substrates.

Furthermore, as **3**, **11**, **13** and **20**, were previously shown to be substrates both of spermine oxidase[37, 38] (SMOX) and acetylpolyamine oxidase[39] (APAOX), it cannot be excluded that **8** and **10**, and/or other of BSAO analogues might be substrate/s of these enzymes, that, producing cytotoxic reaction products, could potentiate the effect of BSAO and to be useful/synergic in the anticancer therapy.

**Table 1.** Molecular structure of PA substrates **1-23** and associated experimental kinetic parameters of BSAO

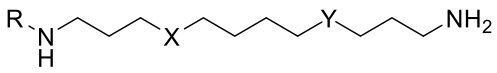


| # PA | R | X | Y | $K_M$ (μM)[a] | $k_{cat}$ ($s^{-1}$)[a] | $k_{cat}/K_M$ ($s^{-1}$ x $\mu M^{-1}$) | Relative $k_{cat}/K_M$ [b] |
|---|---|---|---|---|---|---|---|
| **1** | 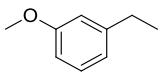 | N | N | 18.6±2.8 | 0.52±0.08 | 0.0280 | 0.06 |
| **2** | 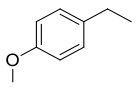 | N | N | 40.7±4.1 | 0.66±0.07 | 0.0162 | 0.03 |
| **3**[c,e] | 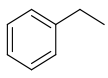 | N | N | 33.9±4.1 | 0.51±0.06 | 0.0150 | 0.03 |
| **4** | 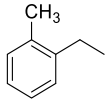 | N | N | 7.2±0.9 | 0.25±0.03 | 0.0347 | 0.07 |

| | | | | | | | |
|---|---|---|---|---|---|---|---|
| **5** | 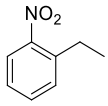 | N | N | 16.8±2.5 | 0.73±0.11 | 0.0435 | 0.09 |
| **6** | 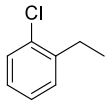 | N | N | 29.7±4.6 | 0.80±0.12 | 0.0269 | 0.06 |
| **7** | 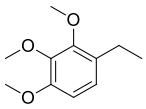 | N | N | 35.0±4.6 | 0.67±0.09 | 0.0191 | 0.04 |
| **8** | 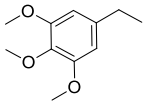 | N | N | 11.0±1.4 | 1.29±0.16 | 0.1173 | 0.25 |
| **9** | 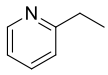 | N | N | 12±1.8 | 0.91±0.14 | 0.0758 | 0.16 |
| **10** | 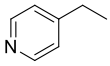 | N | N | 7.2±0.9 | 0.79±0.10 | 0.1097 | 0.23 |
| **11**[d,e] | 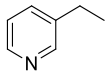 | N | N | 23.8±3.6 | 1.25±0.19 | 0.0525 | 0.11 |
| **12**[d,e] | 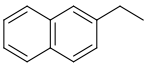 | N | N | 7.8±1.2 | 0.40±0.06 | 0.0513 | 0.11 |
| **13**[d,e] | 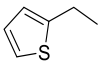 | N | N | 6.0±0.8 | 0.59±0.08 | 0.0983 | 0.21 |
| **14** | 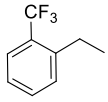 | N | N | 17.0±2.6 | 0.61±0.09 | 0.0359 | 0.08 |
| **15** | 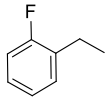 | N | N | 38.0±4.9 | 0.52±0.07 | 0.0137 | 0.03 |
| **16** | 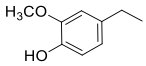 | N | N | 16.2±2.4 | 0.57±0.09 | 0.0352 | 0.08 |
| **17** | 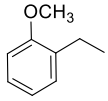 | N | N | 19.8±2.6 | 0.47±0.06 | 0.0237 | 0.05 |
| **18** | H | N | C | 10±1.3 | 0.31±0.04 | 0.0310 | 0.07 |
| **19** | 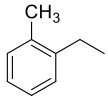 | N | C | 97.0±14.6 | 0.04±0.01 | 0.0004 | 0.00 |
| **20**[e] | 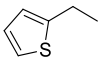 | N | C | 8.4±1.1 | 0.46±0.06 | 0.0548 | 0.12 |

| | | | | | | | |
|---|---|---|---|---|---|---|---|
| **21** | 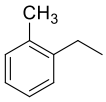 | O | O | 3.8±0.5 | 0.47±0.06 | 0.1237 | 0.26 |
| **22**[c] | 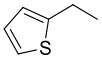 | O | O | 7.0±1.0 | 0.46±0.07 | 0.0657 | 0.14 |
| **23** | H | O | O | 1.6±0.2 | 0.90±0.12 | 0.5625 | 1.20 |
| **Spm** | H | N | N | 3.2±0.46 | 1.5±0.2 | 0.4688 | 1.00 |

[a] Kinetic parameters determined in buffer potassium phosphate 0.01 M at pH 7.6 (T=37°C)

[b]: $k_{cat}/K_M$ of BSAO for Spm, taken as reference substrate, was: 0.469 ±0.050 $s^{-1}$ $\mu M^{-1}$.

[c] **3** = BnSPM.[32, 34]

[d] Compounds previously tested as amine oxidase substrate/inhibitor.[32]

[e] Compounds previously tested as a substrate of amine oxidase.[35]

## Molecular Modeling

### Methodology overview.

To the best of authors' knowledge, only two experimental BSAO structures were available from the protein databank[40] (Figure 2): one co-crystallized with the inhibitor clonidine[21] (CLO, PDB entry code 2PNC) and the free unbound BSAO protein[22] (PDB entry code 1TU5). The co-crystallized structure was employed to select the docking software through a reversible docking assessment procedure. Furthermore, cross-docking experiments[41, 42] were also performed as the BSAO bound topaquinone cofactor[43, 44] (TPQ, 2,4,5-trihydroxyphenylalanine quinone) was observed to have two distinct sidechain conformations in either the CLO bound (2PNC) or the free structure (1TU5). Slightly different TPQ conformations were also visible within the two copies for each BSAO crystal structure (Figure 2).

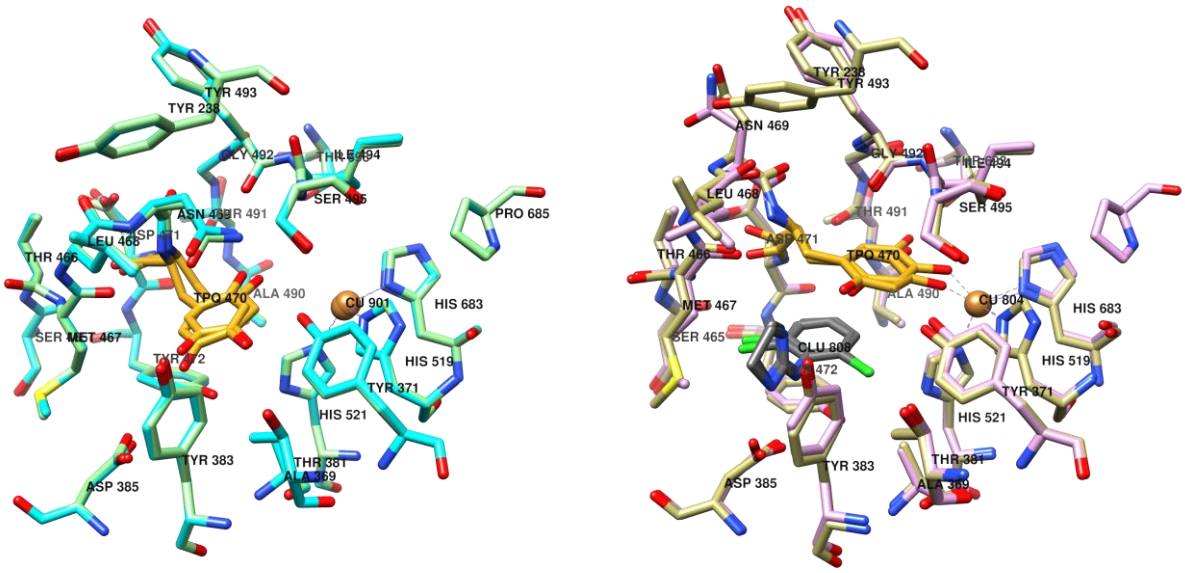


**A** **B**

**Figure 2.** BSAO binding site as experimentally observed in 1TU5 (A) and 2PNC (B) crystal structures. Since two copies of BSAO (chains A and B) for each deposited PDB code were available, both chains are depicted: 1TU5A and 1TU5B are reported in cyan and light green colored carbon atoms, respectively; 2PCNA and 2PCNB are depicted in dark khaki and orchid colored carbon atoms, respectively. Gold and light gray colored carbon atoms indicate TPQ and clonidine (only for 2PNC), respectively. Color codes are referred to those indicated in the UCSF Chimera program.

The docking into free BSAO (1TU5) was performed to confirm the software ability to find low energy poses close to those observed into the inhibited protein (2PNC).

As previously reported,[22] TPQ catalyzes the primary amine substrates oxidation to aldehyde and the concomitant production of hydrogen peroxide through a ping pong mechanism.[4, 45] In particular, in the first half-reaction, the primary amine group reacts with the oxidized TPQ to produce a Schiff-base intermediate and after hydrolysis, there is the release of the aldehyde and TPQ is in its reduced form. In the second half-reaction, the TPQ is re-oxidized by molecular oxygen with the concomitant production of hydrogen peroxide and ammonia (Supporting Information Figure S5).[45] All the compounds we tested have a primary amino group ($R\text{-}CH_2\text{-}NH_2$) and this moiety, which is the reactive one in SPM, can react with the carbonyl moiety of TPQ cofactor during the catalytic cycle. This explains the compounds to behave as substrates (Table 1).

This reaction mechanism, is likely dependent on the TPQ conformational state. Indeed, the two experimental different BSAO sidechain TPQ orientations indicate the *off copper* and *on copper* states[46] as found in 1TU5 and 2PNC, respectively. Regardless of the TPQ orientation, MDock simulations were carried out on PA analogues either by mean of classical reversible molecular docking (RMDock) procedures or with a covalent molecular docking (CMDock) method through covalently binding of Spm and derivatives **1-23** to the TPQ oxygen in position 5. The two docking procedures led to define a series of PAs' aligned datasets that were separated from the proteins and used to build a LB/SB combined CoMFA-like (SB-LB 3-D QSAR) and COMBINE-like models (SB 3-D QSAR) by means of the Py-CoMFA and Py-ComBinE web apps, respectively, both available from the 3d-qsar.com portal.[28, 47] LB 3-D QSAR models were also built from scratch using the PAs' SMILES structures (Figure 3)

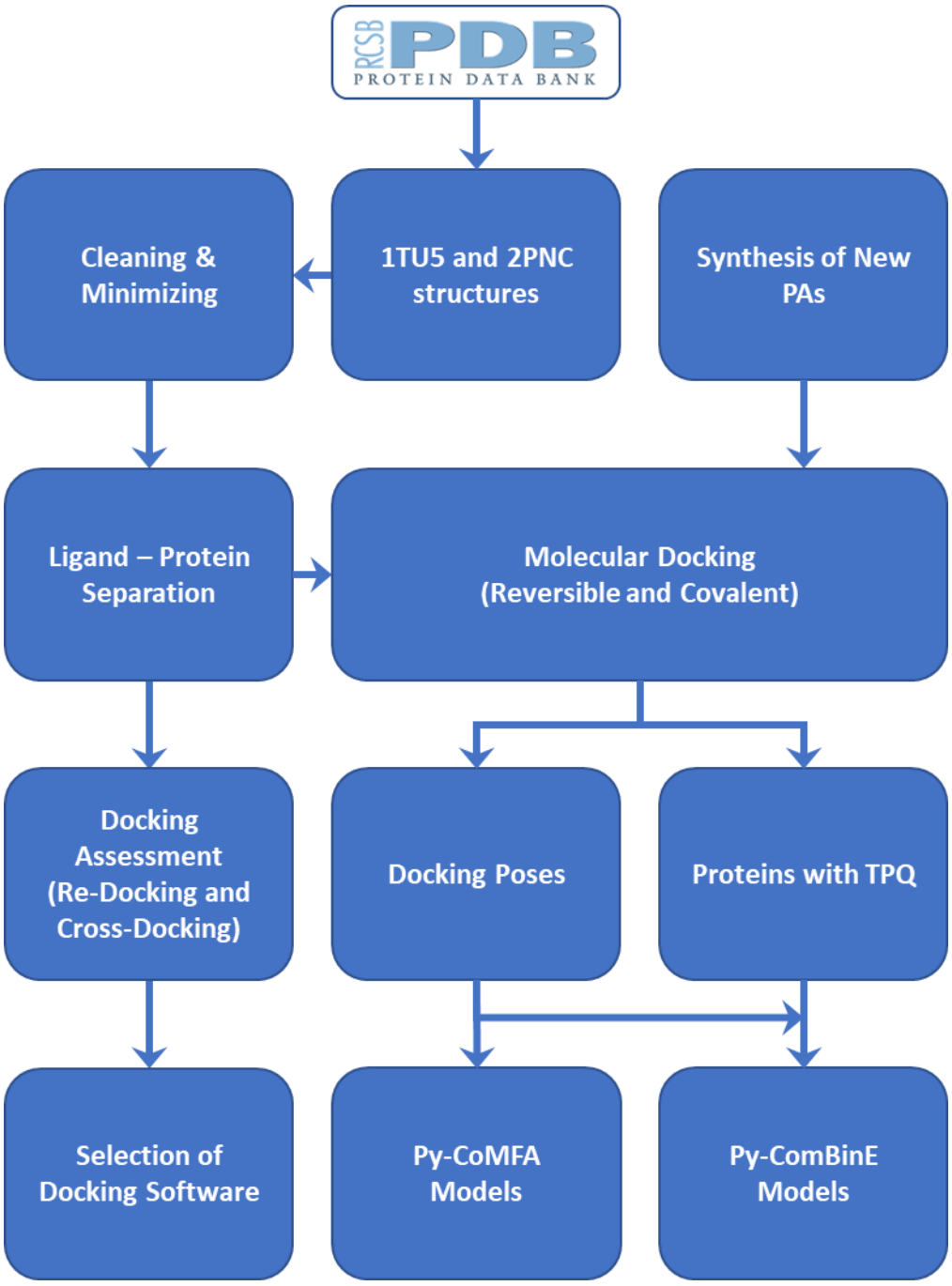


**Figure 3.** General procedure applied in the molecular modeling study.

**RMDock Assessment**

As available within the 3d-qsar.com portal, the programs Smina[48] and Plants[49] were used to assess which software/scoring function combination would result in a lower average root mean square deviation (RMSD) value. As a matter of fact, the cross-docking of clonidine into the free BSAO showed a high RMSD value indicating the drug was not able to correctly bind to the *off copper* BSAO conformation (Table 2 and Supporting Information Tables SI1 and SI2). On the other hand, the RMSD values of redocked clonidine into the *on copper* BSAO conformation confirmed the programs to be able to reproduce, to some extent, the binding conformation of clonidine. In particular, the Plants/PLP program/scoring function combination revealed to be the most effective one with average RMSD values of 1.56 and 0.62 (Table 2). From re-docking experiments it was also evident that clonidine was much better repositioned in the chain A of 2PCN than in chain B.

**Table 2.** RMSD and docking scores values for the docking assessment from clonidine experimental random conformations. Only values for the best performing combination (Plants/PLP) are shown. For the other results see Supporting Information Tables SI1 and SI2.

| Ligand[a] | Conformation[b] | Protein[c] | | | | | | | | Best Docked Lock[c] | Best Docked[f] | | Average[g] RMSD |
|---|---|---|---|---|---|---|---|---|---|---|---|---|---|
| | | 1TU5B | | 1TU5A | | 2PNCA | | 2PNCB | | | | | |
| | | RMSD[d] | Score[e] | RMSD | Score | RMSD | Score | RMSD | Score | | RMSD | Score | |
| 2PNCA | EC | 15.34 | -58.72 | 15.53 | -59.99 | 2.69 | -77.13 | 2.74 | -66.52 | 2PNCA | 2.69 | -77.13 | 1.56 |
| 2PNCB | | 7.86 | -59.58 | 15.12 | -59.19 | 0.42 | -77.04 | 2.48 | -65.91 | 2PNCA | 0.42 | -77.04 | |
| 2PNCA | RC | 12.22 | -61.60 | 11.80 | -62.69 | 0.56 | -79.83 | 2.57 | -67.62 | 2PNCA | 0.56 | -79.83 | 0.62 |
| 2PNCB | | 13.54 | -61.03 | 11.28 | -61.80 | 0.67 | -79.83 | 1.15 | -67.06 | 2PNCA | 0.67 | -79.83 | |

[a]: PDB code from which the CLO ligand was extracted, the last letter indicates the chain.

[b]: EC = experimental conformation; RC = random conformation

[c]: PDB code of the protein used as a receptor, the last letter indicates the chain.

[d]: Root Means Squared Deviation

[e]: PLP score

[f]: RMSD and Score for the best scored docked conformation (low is better)

[g]: Average RMSD value for CLO docking into the 2PNC chains

**RMDock Docking of the tested PAs**

As the Plants/PLP program/scoring function combination was the most effective it was thus applied as a tool to investigate the unbound conformation of the titled PAs into the four BSAO proteins chains extracted from 1TU5 and 2PNC. Although the new PAs should be considered covalent ligands the RMDock could represent a tool to investigate the pre-covalently bound conformations. As expected, and considering that any classical docking program is normally developed to simulate binding for compounds acting as inhibitors the scores for the PAs, working as substrates, were mainly found higher (higher docking energies) for poses docked into the inhibited BSAO *on copper* protein conformation (2PNC) (Supporting Information Tables SI3-SI5). The predicted binding energies therefore indicated the PAs were not able to tightly bind BSAO. At a deeper inspection all of the tested PAs bearing one of the primary amino groups substituted by an aryl methyl group were docked with the aryl methyl head overlapped to the bound clonidine inhibitor (Supporting Information Figure S1). To seek for alternate and more homogeneous binding modes, further RMDock runs were performed into either only 1TU5 chains or only 2PNC chains. Still, many of the PAs docked conformations were found showing the aryl methyl head in the proximity of TPQ in either docking simulations (Supporting Information Figures SI2 and SI3). Among them **7**, **8**, **14**, **16**, **17** docked into 1TU5 protein chains showed a conformation with the primary amino group in the proximity of TPQ residue. These results confirmed the RMDock was not applicable for docking of BSAO substrates. Regarding the docking into only 2PCN chains only **7** and **8** were found to dock with the aryl methyl groups away from the TPQ residues, thus indicating that still the RMDock would not have proposed homogenous docked poses among all the PA derivatives. Regardless the PAs' poses, a direct comparison of the experimental kinetic data ($K_M$ and $k_{cat}/K_M$) with the docking scores revealed the

existence of some correlation (Table 3). In particular among $K_M$ and docking scores a weak negative correlation was observed, while a strong direct correlation was calculated among $k_{cat}/K_M$ and the docking scores (Table 3).

**Table 3.** RMDock energies in comparison with the experimental kinetic data $K_M$ and $k_{cat}/K_M$

| PA[a] | $K_M$ | $k_{cat}/K_M$ | Best Docked Score[b] | 2PNC Best Docked Score[c] | 1TU5 Best Docked Score[d] |
|---|---|---|---|---|---|
| **1** | 18.60 | 0.0280 | -113.23 | -113.34 | -101.73 |
| **2** | 40.70 | 0.0162 | -109.81 | -113.16 | -108.63 |
| **3** | 33.90 | 0.0150 | -113.26 | -111.05 | -111.44 |
| **4** | 7.20 | 0.0347 | -114.93 | -115.17 | -100.43 |
| **5** | 16.80 | 0.0435 | -116.98 | -114.84 | -99.72 |
| **6** | 29.70 | 0.0269 | -112.10 | -114.86 | -102.90 |
| **7** | 35.00 | 0.0191 | -106.21 | -104.75 | -100.81 |
| **8** | 11.00 | 0.1173 | -110.91 | -109.25 | -102.73 |
| **9** | 12.00 | 0.0758 | -104.21 | -105.57 | -104.83 |
| **10** | 7.20 | 0.1097 | -106.64 | -109.14 | -102.96 |
| **11** | 23.80 | 0.0525 | -106.13 | -107.63 | -103.46 |
| **12** | 7.80 | 0.0513 | -118.46 | -115.55 | -112.28 |
| **13** | 6.00 | 0.0983 | -103.97 | -103.66 | -103.59 |
| **14** | 17.00 | 0.0359 | -115.50 | -114.41 | -103.28 |
| **15** | 38.00 | 0.0137 | -112.71 | -115.61 | -113.15 |
| **16** | 16.20 | 0.0352 | -119.50 | -115.56 | -102.43 |
| **17** | 19.80 | 0.0237 | -113.34 | -113.17 | -101.79 |
| **18** | 10.00 | 0.0310 | -87.63 | -83.03 | -87.67 |
| **19** | 97.00 | 0.0004 | -117.29 | -116.03 | -108.35 |
| **20**[e] | 8.40 | 0.0548 | -109.92 | -107.70 | -103.75 |
| **21** | 3.80 | 0.1237 | -114.66 | -112.71 | -107.13 |
| **22** | 7.00 | 0.0657 | -105.63 | -105.24 | -104.12 |
| **23** | 1.60 | 0.5625 | -81.44 | -76.55 | -81.12 |

| | | | | | |
|---|---|---|---|---|---|
| **Spm** | 3.20 | 0.4688 | -82.78 | -77.44 | -83.07 |
| Pearson correlation coefficient with $K_M$ | | | -0.35 | -0.37 | -0.41 |
| Pearson correlation coefficient with $k_{cat}/K_M$ | | | 0.77 | 0.80 | 0.76 |

[a]: number of polyamine structure

[b]: the best score from cross-docking experiments into the four chains

[c]: the best score from cross-docking experiments into only 2PNC chains

[d]: the best score from cross-docking experiments into only 1TU5 chains

**CMDock Docking of the tested PAs**

Since the PAs proved to act as BSAO substrates, they would undergo a covalent interaction with the TPQ, making a Schiff intermediate before the oxygen activation and the subsequent oxidation of the imine (Supporting Information Figure S5).[45, 50, 51] This mechanism was observed for the imidazole and 2-hydrazinopyridine bound to TPQ in the human semicarbazide-sensitive amine oxidase (SSAO, PDB entry code 2Y74)[52] and in the vascular adhesion protein-1 (VAP1, PDB entry code 2C11).[53] Following the PA oxidation mechanism (Supporting Information Figure S5) a CMDock protocol was set up to investigate the possible mechanism of interaction between BSAO and the titled PAs (Figure 4).

In the CMDock procedure an overall mimicking of the reversible PA-TPQ adduct formation was simulated in discrete steps, thus the PAs' covalent docked conformations were subsequently dissociated in two steps: a first local minimization of the unbound PAs and a second one using a reconstituted TPQ structure.

First, each PA was modeled from its SMILES structure and covalently linked to the TPQ, deprived of the oxygen in position 5, to form a TPQ-PA adduct residue, taking care of the proper protonation state in agreement with the experimental assay conditions (covalent docking step 1 in Figure 4). Then, by means of the latest version of Vina software[54] a water molecule was docked while letting the TPQ-PA adduct to flexibly move. Either the vina[54] or vinardo[48] scoring functions were used during the CMDock and were also used to re-score each separated PAs docked conformations leading to furnish two covalently docked molecule datasets ($PA_{Cov\text{-}Vinardo}$ and $PA_{Cov\text{-}Vina}$) to be used

as training set in the subsequent 3-D QSAR modeling (covalent docking step 2 in Figure 4). Subsequently, each PA was unbound from the respective TPQ adduct and the complex minimized, through the Smina docking software minimization feature, while keeping the TPQ deoxygenated in position 5, to avoid atoms overlapping. This process mimicked the formation of the C=N Schiff base double bond (dissociation step 1 in Figure 4) in agreement with the experimental covalently bound 2-hydrazinopyridine as found in the SSAO.[52] The best energy scored minimized PAs furnished a further couple of datasets ($PA_{Min1\text{-}Vinardo}$ and $PA_{Min1\text{-}Vina}$) to be used as a training set to build either 3-D QSAR or COMBINE models (with the associated protein counterpart). Then a second Smina minimization round was performed after the reconstitution of the full TPQ structure leading to the $PA_{Min2\text{-}Vinardo}$ and $PA_{Min2\text{-}Vina}$ datasets as 3-D QSAR and COMBINE training sets (dissociation step 2 in Figure 4). Two further COMBINE training sets were also compiled using the unminimized TPQ containing BSAOs and the $PA_{Min1\text{-}Vinardo}$ and $PA_{Min1\text{-}Vina}$ mimicking the reacting PA with the TPQ oxygen in position 5 ($PA_{Min3\text{-}Vinardo}$ and $PA_{Min3\text{-}Vina}$) thus mimicking the close detachment/attachment of the PA from the deoxygenated TPQ. The procedure was repeated for each of the four chains available from the 1TU5 and 2PNC crystal structures.

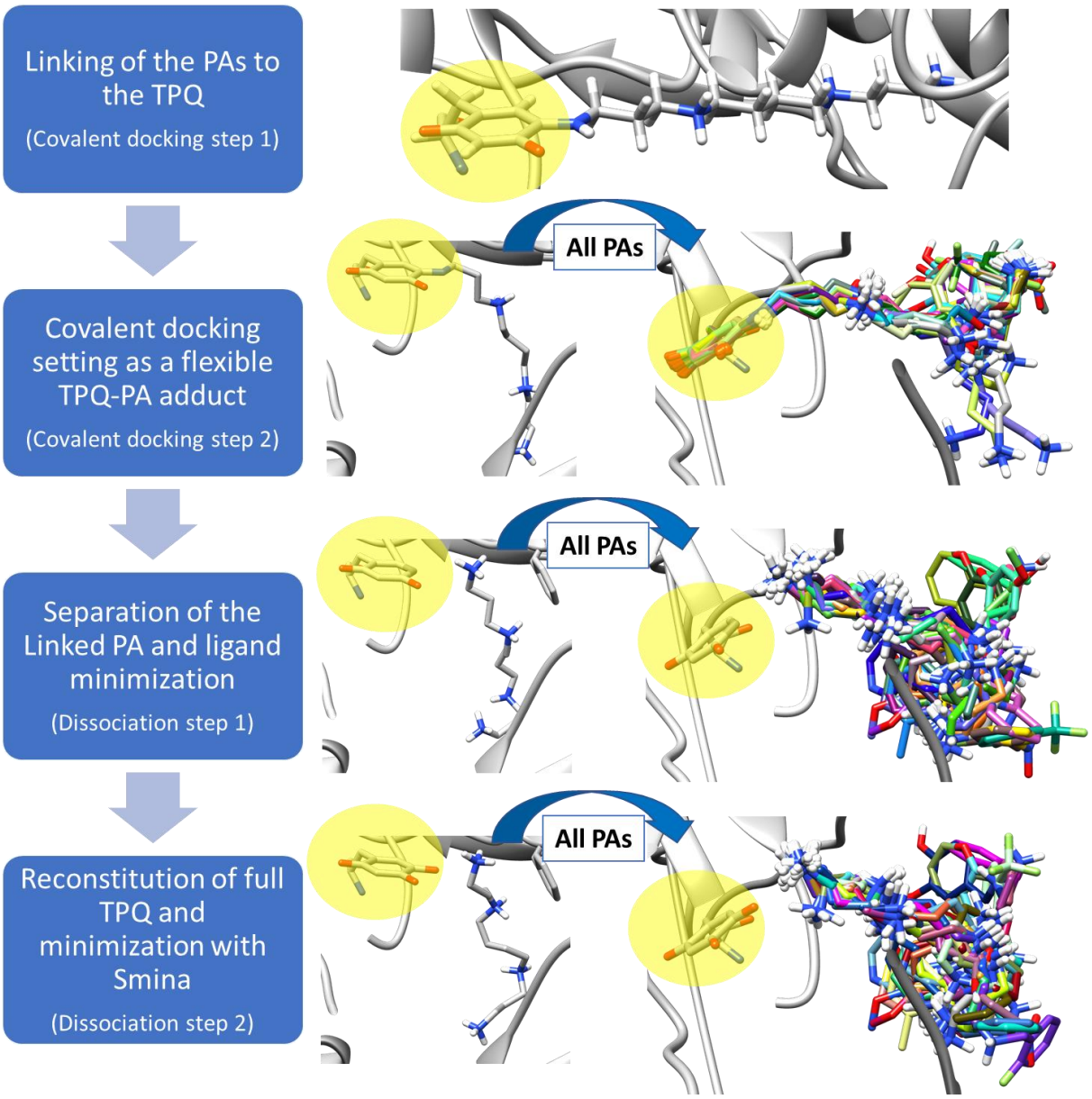


**Figure 4.** Workflow of the CMDock procedure and the subsequent minimizations of the covalently docked PAs. The Spm is shown as an example for a given PA. Conformations of Dissociation step 1 were merged into BSAO with fully reconstituted TPQ (highlighted with a yellow shadow) (see main text).

Inspection of proposed docked poses obtained applying two scoring functions (vina and vinardo) in the four available chains displayed eight different scenarios. Only the CMDock with the vinardo scoring function in the chain A of 1TU5 led to poses all docked in the same area as well as all the

TPQ oriented in the same direction (Figure 5 and Supporting Information Figure S4). The orientation of the TPQ was consistent with the *off copper* state (1TU5) observed in the free BSAO crystal structure and overlapped to that of the 2-hydrazinopyridine/TPQ adduct as found in the SSAO complex[52] (2C11).

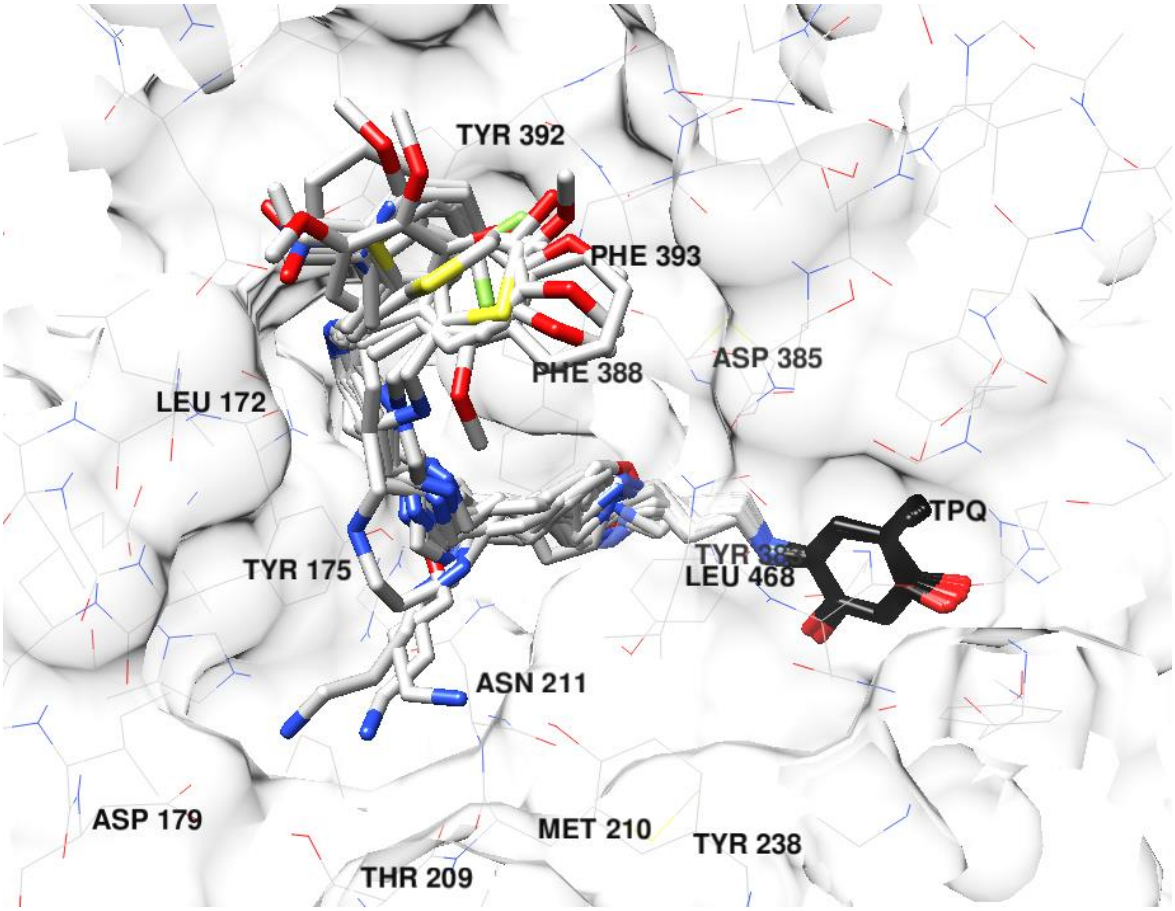


**Figure 5.** PAs covalent binding mode proposed by the Vina program and selected by a rescore with the vinardo scoring function using the CMDock procedure. In black the TPQ and light gray the chain A of 1TU5 residues and its 80% transparent surface.

The aryl heads of all covalently docked rescored arylmethyl derivatives **1-17** and **19-22** were observed to bind in a hydrophobic pocket formed by Leu172, Tyr175, Glu417, Tyr392 and Phe393 sidechains, while compounds **18**, **23** and Spm, without any arylmethyl moiety at the terminal

primary amino groups, were all found in a different pocket mainly formed by Asp179, Thr209, Met210, Asn211, Phe226 and Tyr238. Clearly the primary amino group capped with the aryl methyl somehow has a definite influence in the binding mode of PAs. For compounds **18**, **23** and Spm the main driving force are the hydrogen bonds taking place between their terminal amino groups and Thr209 and Tyr238 hydroxyls (Figure 6A).

Notably, compound **21** showed a BSAO affinity comparable to that of Spm, nevertheless from a simple analysis of steric contacts no particular feature or interaction could be associated with its potency. The only difference with all the other arylmethyl derivatives is the 2-methyl group and the oxygen bridge better hosted in the small hydrophobic tube formed by Tyr175, Tyr383, Phe388, Phe393 and Leu468 (Figure 6A). A slightly different scenario was observed after the minimization with Smina in which the role of Tyr238 was of greater importance for PA/BSAO molecular recognition. From the two sequential minimizations of dissociated PAs, it seems that Tyr238 would represent the main anchor point to drive the substrates to the subsequent covalent binding to TPQ (Figure 6B). This observation was particularly consistent for nine out of ten compounds (Spm, **4**, **10**, **12**, **13**, **18**, **20**, **21** and **23**) characterized by $K_M$ values up to 10 μM (not shown).

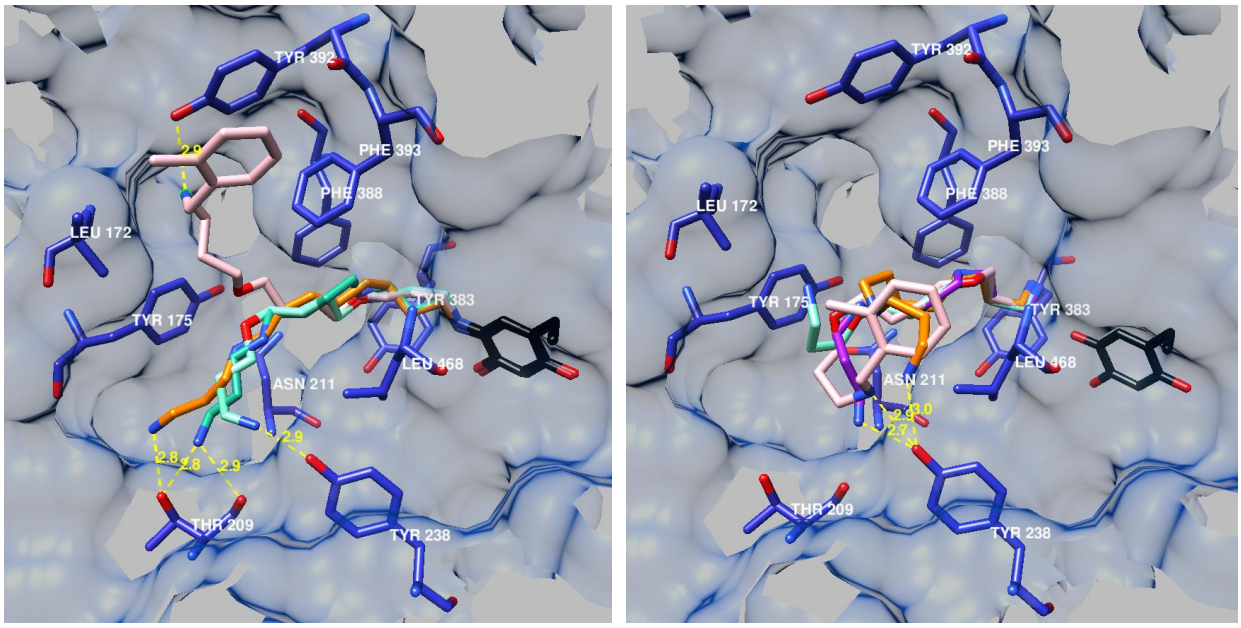


**A** **B**

**Figure 6**. Spm (green in A and purple in B), **18** (orange), **21** (pink)and **23** (aquamarine)binding mode proposed by the Vina program and selected by a rescore with the vinardo scoring function using the CMDock procedure. In panel A, the conformations bonded to the TPQ. In panel B the conformations after two local minimizations with Smina (last step in Figure 4). The chain A of 1TU5 residues and its 80% transparent surface were depicted in dodger blue. In black the conformation of TPQ as found during the CMDock procedure.

## 3-D QSAR Modeling

**General procedure**.

3-D QSAR models were built by means of the Py-CoMFA web app available from the 3d-qsar.com freely accessible portal either starting from the PAs' SMILES structures (Full LB models) or from their docked conformations obtained from either the RMDock or the CMDock procedure above described (Mixed LB-SB models) (Figure 7).

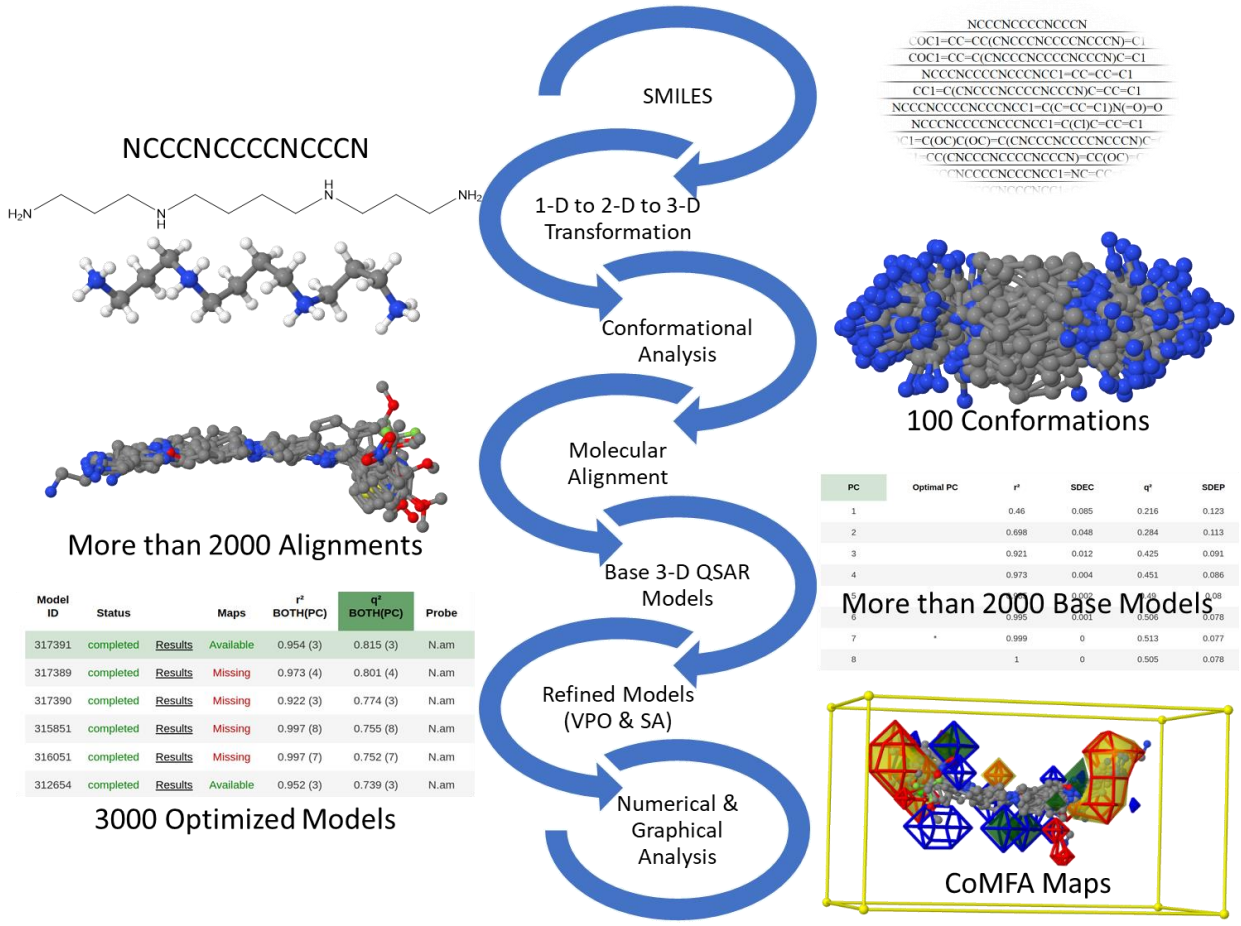


**Figure 7.** Workflow to build the 3-D QSAR models. LB models started from SMILES structures, while SB started directly from the "Default 3-D QSAR Models" step.

## Full Ligand-Based Models

The Full LB models were built by first seeking for the best alignment rule through a series of eleven conformational analyses run on all PAs.[55] Then for each conformational analysis 32 different molecule templates and 6 combinations of alignment software settings led to 2112 molecular alignments used to build 2112 Py-CoMFA models using the default settings (see experimental section). The procedure was applied to either $pK_M$ ($-\log_{10}[K_M]$) or $p(k_{cat}/K_M)$ ($-\log_{10}[k_{cat}/K_M]$) values as dependent variable (Table 1). The model (LB1, Table 4) endowed with the highest $q^2$ value (0.47 at 5 principal components, Supporting Information Table S6) was obtained using the $pK_M$ values, conformational analysis calculated with the balloon software[55] using the MMFF94 force field and aligned by means of RDKit library (http://www.rdkit.org) using

the "Best Score" alignment scoring function. As template molecules the one with highest LogP value (**19**, LogP = 3.364) in its longest conformation (Supporting Information Table S7 and Figure S6) was used. Using the $pk_{cat}/K_M$ activity value a maximum $q^2$ value of 0.41 was reached.
Model LB1 was optimized by running 3000 random variable pretreatment optimizations (VPO, Supporting Information Figure S7) to furnish model LB2, selected based on highest $q^2$ (0.74) and lowest number of optimal PCs (3) (Table 4, Supporting Information Table S8) obtained with the amidic probe atom (N.am) and charge model, minimum sigma, grid spacing, dielectric constant and cutoff of MMFF94, 0.8, 2.7, 1.0, 3 and 2.0, respectively (Supporting Information Table S9). The final LB3 model (Table 4, Supporting Information Tables SI10 and SI11) was obtained by means of a simulated annealing (SA) feature selection and characterized by a $q^2$ value of 0.82 with significant increments of 74% and 11% with respect to LB1 and LB2 models.

**Table 4.** LB1, LB2 and LB3 Py-CoMFA models' statistical coefficients. LB1, LB2 and LB3 models are related each to the other as the training set alignment is the same. LB1 was the best initial model. LB2 and LB3 were derived from LB1 by mean of a model optimization by VPO and SA feature selection.

| #[a] | Probe Atom[b] | # PCs[c] | $r^2$ [d] | SDEC [e] | $q^2$ [f] | SDEP [g] |
|---|---|---|---|---|---|---|
| LB1 | N.am | 5 | 0.99 | 0.01 | 0.47 | 0.08 |
| LB2 | N.am | 3 | 0.95 | 0.01 | 0.74 | 0.04 |
| LB3 | N.am | 3 | 0.95 | 0.01 | 0.82 | 0.03 |

[a]: model ID

[b]: atom to calculate the molecular interaction fields

[c]: optimal number of PLS principal components

[d]: squared correlation coefficient

[e]: Standard error of calculation by the model

[f]: cross-validated squared correlation coefficient

[g]: Standard error of prediction during cross-validation

Model LB3 was analyzed by inspecting the CoMFA-like maps obtained by the product of the PLS coefficients (Coeffs) by the average molecular interaction field (MIF) values to give the average

activity contribution (AAC) maps for either steric (STE) or electrostatic (ELE) MIFs (Supporting Information Figure S9). Although model LB3 was of outstanding statistical levels being the model built on highly closely related compounds the associate AAC maps were of low utility. The most important characteristic that LB3 model highlighted relates to the length of the molecules. In fact, arylmethyl head bearing PAs' are longer than those with unsubstituted two primary amine groups. This was clearly underlined by the Py-CoMFA yellow polyhedrons (STE negative AAC, panel A and C of Supporting Information Figure S9) that resided on top of the molecules' ends. While compound **23** did not overlap the above polyhedrons, the lowest active derivative (**19**) being longer than **23** extended both ends over the two yellow polyhedrons. This would suggest that the aryl methyl heads should not be used as substituents leading to longer molecule, but instead as replacements of the propylamino groups of both Spm and **23** so to keep as much as possible their molecule length. On the other hand, a few small green polyhedrons (positive $AAC_{STE}$) are around the overlapped molecules (not shown) without a clear indication on which possible substitution could exert some influence on $pK_M$. These observations thus suggested that to expand the model applicability some branched PA should also be investigated.

Regarding $AAC_{ELE}$ maps, similarly to $AAC_{STE}$, the most important polyhedrons were the two red on the extremities of the molecules indicating the importance of a hydrogen bond donating group in those regions (panel B and D of Supporting Information Figure S9). While one end largely satisfied these requirements, the ends corresponding to the aryl methyl head were mostly highly hydrophobic and lacked of hydrogen bond donor groups. Some compounds partially filled this lack with the presence of heteroatoms or hydroxyl groups (i.e. **10** or **16**), therefore it could be speculated that the insertion of more than one hydroxyl or even an aminomethyl group would likely lead to a better biochemical kinetic profile.

**Ligand-Based and Structure-Based Mixed Models**

From the PA analogues docking results,a series of SB-aligned datasets were obtained and promptly uploaded into the 3d-qsar.com portal to build 3-D QSAR model with the same protocol applied to already aligned molecules.[28] Default Py-CoMFA models were built for the RMDock datasets, using either $pK_M$ or $pk_{cat}/K_M$, but none of them showed satisfying $q^2$ values and therefore were not further investigated. A different scenario was observed for the six datasets ($PA_{Cov\text{-}Vinardo}$, and

$PA_{Cov\text{-}Vina}$, $PA_{Min1\text{-}Vinardo}$, $PA_{Min1\text{-}Vina}$, $PA_{Min2\text{-}Vinardo}$ and $PA_{Min2\text{-}Vina}$) obtained with the CMDock procedure (Figure 4). In agreement with both the LB models and docking results, acceptable models were only obtained (data not shown) using $pK_M$ and the PA conformations docked using the vinardo scoring function (Figure 5) obtained within the above described dissociation step 1 (Figure 4). Therefore, the $PA_{Min1\text{-}Vinardo}/pK_M$ dataset was subjected to the same Py-CoMFA procedure described above (Figure 7) by skipping the alignment steps. Therefore after 3000 random VPO optimizations (Supporting Information Table S12) the top three different models were further investigated by SA feature elimination to select the model characterized by the amidic atom probe (N.am) and charge model, minimum sigma, grid spacing, grid extension, dielectric constant and cutoff of qeq, 0.4, 2.9, 5, 59 and 28, respectively (Supporting Information Tables SI12-SI14 and Figure S10). Being aligned by a SB method the Py-CoMFA model associated maps can be directly interpreted overlapped to the BSAO binding site to combine the docking results with the 3-D QSAR data (Figure 8). This kind of overlapping clearly shows the convergence of the two techniques (CMDock and 3-D QSAR). Taking as references Spm and **19** as the highest affinity and lowest processed substrates, respectively, the $AAC_{STE}$ (Figure 8A) and the $AAC_{ELE}$ (Figure 8B) polyhedrons were found in agreement with the above discussed binding mode. In particular, Spm was mainly surrounded by green polyhedron (positive $AAC_{STE}$) and the largest one was actually indicating as important for the Spm-Tyr238 interaction. On the other hand, a big yellow (negative $AAC_{STE}$) polyhedron greatly overlapped to the **19** benzylaminopropyl portion while fulfilling the hydrophobic pocket formed mainly by Leu172, Phe388, Tyr392 and Phe393 residues. Regarding the $AAC_{ELE}$ plot, a small blue polyhedron highlighted the hydrogen bond between the Spm primary amino group and the Tyr238 hydroxyl moiety, other blue spots were also visible, but no specific association can be done. Differently, a big red polyhedron run over the big yellow one, thus indicating that not only the occupation of that portion was negatively associated with the $pK_M$ but also that hydrogen donating groups could enhance the biological activity, in agreement with the full LB models.

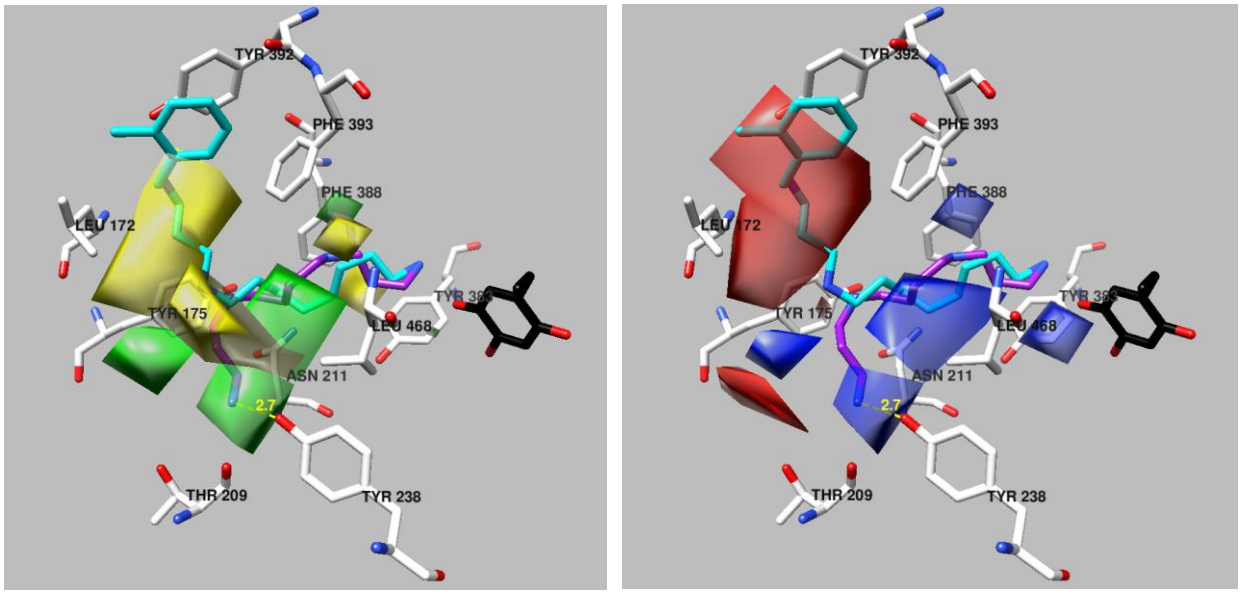


**Figure 8**. SB 3-D QSAR model AAC maps overlapped to the 1TU5 chain A (white). In panel A the $AAC_{STE}$ plot overlapped to Spm (purple) and **19** (cyan). In panel B $AAC_{ELE}$ plot. In black is also represented the reconstituted TPQ after the separation of the covalently docked PA. The polyhedrons represent the AAC obtained by the product of the PLS coefficients with the average MIF values.

## COMBINE Models

Differently from the above CoMFA-like 3-D QSAR approaches (Py-CoMFA), COMBINE represents a full SB 3-D QSAR where the descriptive variables (regression parameters) are represented by the ligand/protein interactions on a per residue basis energy deconvolution. Therefore, as the $PA_{Min1\text{-}Vinardo}/pK_M$ dataset showed some agreement among the docked conformations and the built over SB/LB 3-D QSAR model a COMBINE approach was therefore applied utilizing the Py-ComBinE web app available on the www.3d-qsar.com website. The COMBINE model was built by combining the **1-23** and **Spm** docked conformations with the BSAO containing the reconstituted TPQ as above described in the covalent docking procedure before running the second Smina minimization to produce the $PA_{Min2\text{-}Vinardo}$ dataset. For a complete description of the ligand/BSAO recognition playing forces, four types of ligand/protein interactions were calculated: van der Waals (STE), coulombic (ELE), desolvation (DRY) and

hydrogen bonding (HB) and correlated through the partial least square (PLS) to the $pK_M$ values' vector. To reduce data redundancy, the optimal PLS model was carried out through a SA feature selection leading to a COMBINE model characterized by $r^2$, SDEC, $q^2$ and SDEP values of 0.87, 0.14, 0.62 and 0.25, respectively (Table 5 and Supporting Information Table S15 and Figure S11).

**Table 5.** Py-ComBinE model statistical coefficients.

| # PC | $r^2$ [b] | SDEC [c] | $q^2$ [d] | SDEP [e] | SDEP Decrement |
|---|---|---|---|---|---|
| 1 | 0.37 | 0.31 | 0.17 | 0.36 | |
| 2 | 0.65 | 0.24 | 0.36 | 0.32 | 11.91% |
| 3 | 0.83 | 0.17 | 0.46 | 0.29 | 8.49% |
| 4[a] | 0.87 | 0.14 | 0.62 | 0.25 | 15.46% |
| 5 | 0.88 | 0.14 | 0.59 | 0.25 | -2.85% |

[a]: optimal number of PLS principal components

[b]: squared correlation coefficient

[c]: Standard error of calculation by the model

[d]: cross-validated squared correlation coefficient

[e]: Standard error of prediction during cross-validation

Analogously as for the above CoMFA models, per residue AAC were generated by multiplying each interaction energy by the associated PLS coefficients ($AAC_{STE}$, $AAC_{ELE}$, $AAC_{DRY}$, $AAC_{HB}$, Figure 9). A strong negative $AAC_{ELE}$ was found to be associated with Asp385 indicating that the lack of interaction with that residue reduces the affinity of about 0.2 $pK_M$ units. This interaction is connected to the TPQ interacting amino group, therefore an optimal distance would ensure the correct formation of the covalent bond. Effective substrates such as compound **23** and Spm showed a distance of 2.7 Å between the primary amino group nitrogen and the Asp385 delta oxygen atom. Longer distances were observed for less efficient substrates such as **2** (2.8 Å), **5** (2.8 Å), **15** (2.8 Å), **19** (2.8 Å) and **20** (2.9 Å) (not shown). Negative $AAC_{STE}$ of about 0.01-0.05 $pK_M$ units were associated with Thr209, Tyr238 and Phe388. As above discussed Thr209 and Tyr238 were already recognized as important residues for hydrogen bonding (Figure 6), therefore any interaction not electrostatic-like would not have been well accepted. In fact, a positive $AAC_{ELE}$ of 0.02 $pK_M$ units

was also associated with Tyr238. Phe388 was already depicted to participate in the shape fitting of the docked PAs and the rigid nature of the COMBINE method cannot account exactly for its role. A positive $AAC_{STE}$ of almost 0.04 $pK_M$ units was associated with Tyr175 which was above recognized as an important residue in hosting the PAs' heads. Regarding $AAC_{DRY}$, a notably positive value was observed for Tyr175 that summed to the $AAC_{STE}$ further highlights its role for non-electrostatic type interactions, also supported by the lack of any $AAC_{ELE}$ or $AAC_{HB}$. Met210 follows the same tendency as Tyr175 and its hydrophobic contributions are congruent with the full LB and mixed LB/SB studies (Figure 10). A different profile was instead found for Thr209 whose low $AAC_{STE}$ and $AAC_{DRY}$ values supported its role for ELE or HB type interactions.

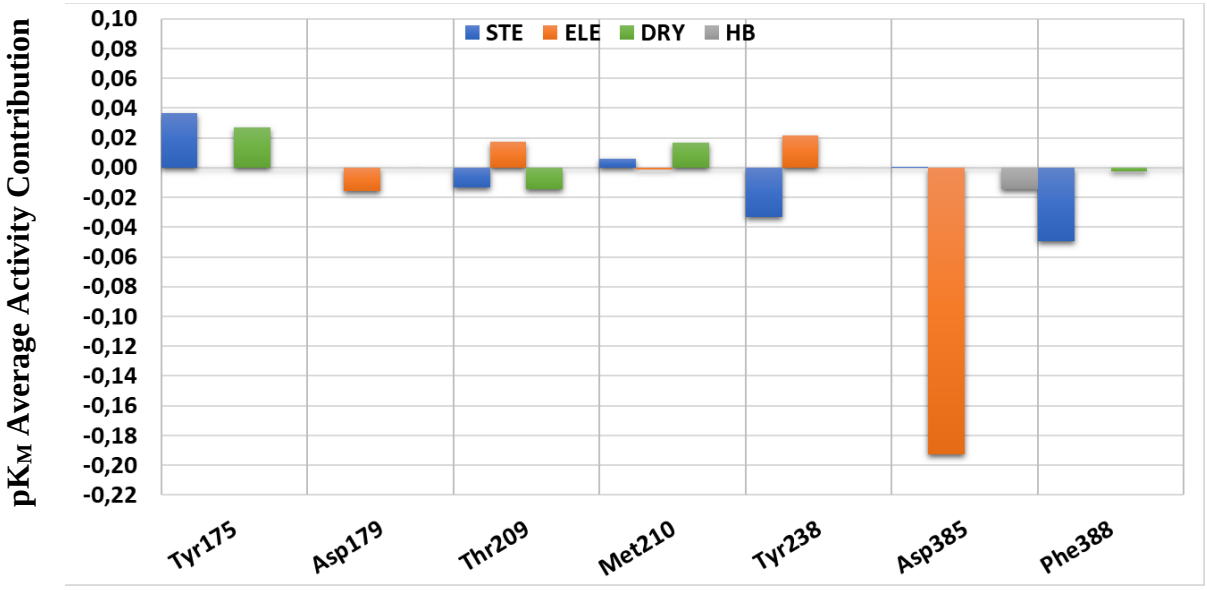


**Figure 9**. AAC plot for the COMBINE model. To reduce redundancy values were filtered at 0.01 activity contribution.

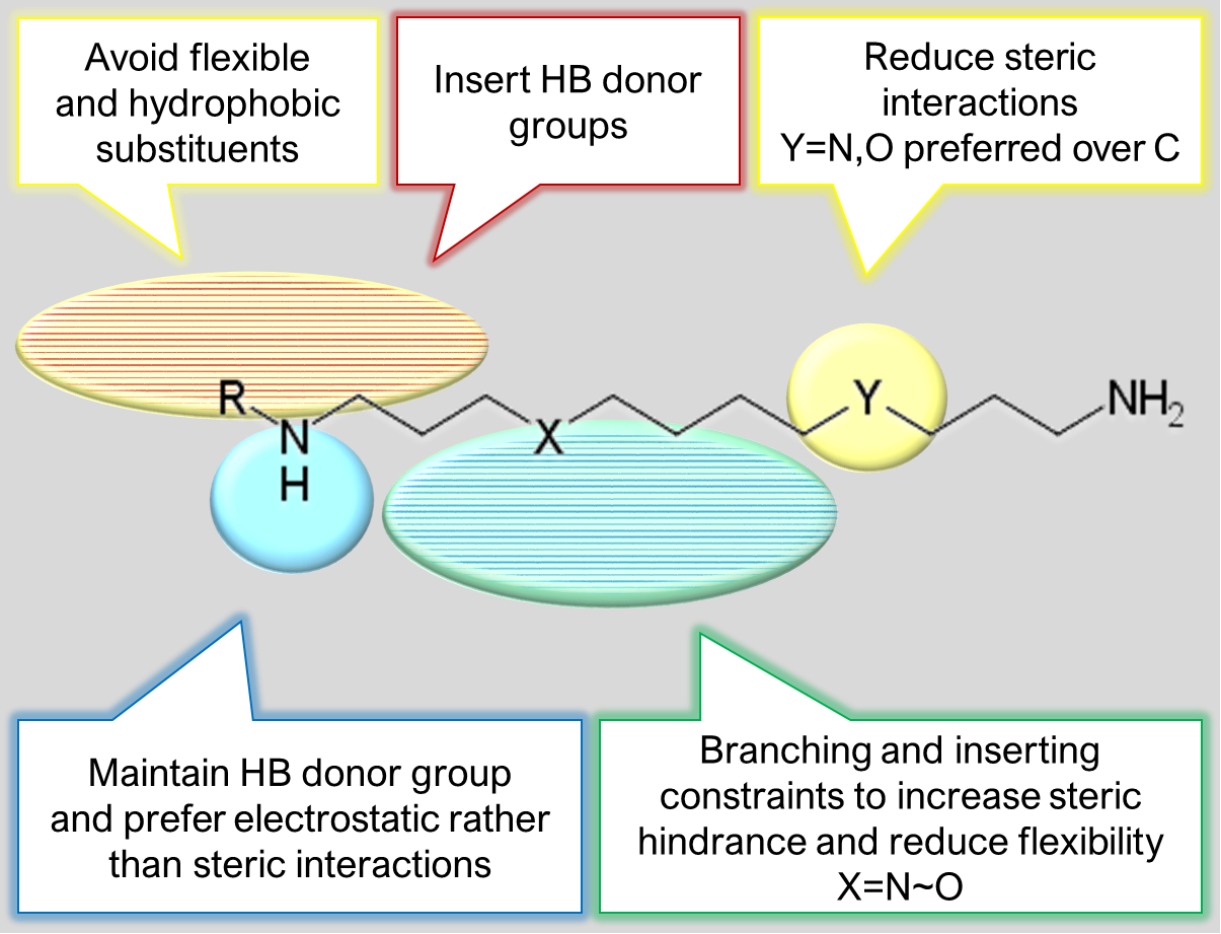


**Figure 10**. Overall 3-D SAR of Full LB, LB/SB 3-D QSAR and COMBINE models. Circles are color-coded to represent steric (favorable green, unfavorable yellow) and electrostatic (favorable blue, unfavorable red) features, as in Figure 8. Striped two-colored circles account for two features together.

**Summary of the main conclusions from the molecular modeling studies**

Reversible docking (RMDock protocol) showed the PA uniformly binding into BSAO with conformations resembling an inhibitor, notwithstanding their energies of docking as predicted by the vinardo scoring function were found in good agreement with the $K_M$ values, indicating that this tool could be used to fast screen other substrates to subject to deeper molecular modeling investigations. Interestingly the CMDock procedure was applied in a fashion to simulate the formation/dissociation of the Schiff base, the first step of the BSAO catalytic mechanism.[45] The Vina program with the vinardo scoring function was the selected combination as during the

covalent docking was the only one proposing a uniform series of docked conformations. Inspection of the covalently docked PAs indicated that substrates bearing a second free primary amino group preferred bindings slightly different than those bearing an aryl methyl substituent on the amino termini. Short branched derivatives could couple the two binding modes likely leading to better substrates or BSAO ligands.

The $pK_M$ derived LB 3-D QSAR was useful to state that the optimal substrate should not be too longer than that of the natural substrate Spm. Furthermore, in agreement with the binding mode analysis, the model also suggested that branched derivatives should be designed to expand the model applicability. The LB model could represent a second filter in a virtual screening campaign. A different scenario was observed with the LB-SB mixed 3-D QSAR, obtained with the $pK_M$ values and ligand conformations through the covalent docking procedure. In particular the conformations related to the first minimized dissociated covalently docked PAs furnished the best model. The statistical coefficients goodness suggests that the model could be used as a third filter to select compounds likely able to covalently bind the TPQ similarly as previously reported.[56] As last, modeling investigation a COMBINE model was developed as a final selection tool for new potential BSAO substrates. As the method associated docking and SB 3-D QSAR[57, 58] it implies the highest level of investigation that could lead to the selection/design of new potential BSAO substrates. Inspection of the Py-ComBinE model derived on the $PA_{Min3\text{-}Vinardo}$ dataset gave insights on the substrate/BSAO residue interactions to be avoided or maintained for future designed PA derivatives.

## Conclusions and perspectives

A series of new Spm derivatives along with recently reported analogues was herein investigated as BSAO substrates to derive a tool to be applied in the design of compounds to potentially be used in a future anticancer therapy. BSAO as an enzyme that oxidatively deaminates natural PAs while freeing *in situ* cytotoxic compounds ($H_2O_2$ and aldehydes) known to induce cancer cell death.

From the experimental biological assays results, new effective BSAO substrates emerged among the tested analogues. In particular, compared to the physiological Spm, BSAO showed relevant levels of catalytic constant, efficiency and affinity values for **8** and **10**, **13** (with a Spm skeleton),

**21** and **23** (a diamine derivative). As **3**, **11**, **13** and **20**, were previously found to be also substrates for either SMOX or APAOX,[39] it cannot be excluded that also **8** and **9**, and/or other analogues might be substrates for APAOX and/or SMOX and consequently could potentiate the effects in an eventual anticancer therapy.

The experimentally kinetic parameters ($K_M$ and $k_{cat}$) of the studied compounds were used in LB and SB applications (CMDock, 3-D QSAR and COMBINE) as tools to define 3-D structure-activity relationships for the future design of new BSAO substrates.

Molecular docking combined with LB and SB 3-D QSARs suggested that short branched derivatives could lead to better substrates or BSAO ligands.

In conclusion, this study represents the first application of a combination of molecular modeling procedures that could be used for the design of novel BSAO substrates with potential future pharmacological application.

Future perspective will be a further investigation on the novel BSAO substrates here found (**8, 10**, **13**, **21** and **23**) and on new designed substrates on the basis of the MDock combination with 3-D QSARs studies to evaluate their cytotoxic effect also in combination with nanoparticles as drug-delivery system in anti-cancer therapies. In particular, the conjugation of core–shell nanoparticles with BSAO is a new approach to immobilize this copper-enzyme on gold-polymer nanosystems stabilized by a hydrophilic macromolecule. The conjugated BSAO-nanoparticles coupled with novel substrates could have several applications in pharmaceutical fields, as a biosensor, and in medicine as anti-cancer therapy.[16, 19]

## Experimental section

### Chemistry

The chemicals were analytical grade. Purified bovine serum amine oxidase was prepared as previously reported.[17, 18, 44] All the commercially available reagents and solvents were purchased from Sigma-Aldrich (St. Louis, MO, USA), Alpha Aesar (Haverhill, MA, USA), VWR (Radnor, PA, USA), and TCI, which were used without further purification. Reactions were followed by analytical thin layer chromatography (TLC) on precoated TLC plates (layer 0.20 mm silica gel 60 with a fluorescent indicator UV254, from Sigma-Aldrich). Developed plates were air-dried and analyzed under a UV lamp (UV 254/365 nm), KMnO4stain. Nuclear magnetic resonance (NMR)

experiments were run on Varian VXR 400(400 MHz for1H, 100 MHz for13C). Chemical shifts (d) are reported in parts per million (ppm) relative to tetramethylsilane (TMS) as an internal reference and coupling constants (J) are reported in hertz (Hz). The spin multiplicities are reported as s (singlet), br s (broad singlet), d (doublet), t (triplet), q (quartet), and m (multiplet). Mass-spectra were recorded on a VG707EH-F apparatus, and electrospray ionization (ESI) both in positive and negative mode was applied. Compounds were named following IUPAC rules as applied by ChemBioDraw Ultra (version 17.0). All of the final compounds showed 95% purity by elemental analysis.

**General procedure for the synthesis of 24-31 and 33-34.**

A solution of tri-Boc-spermine (0.502 g, 1 mmol) and the appropriate aldehyde (1.1 mmol) in toluene (25 ml) was refluxed in a Dean-Stark apparatus for 3 h. After cooling, the solvent was removed in vacuo, the residue was taken up in EtOH (30 ml) and $NaBH_4$ (0.151 g, 4 mmol) was added to a cooled (0 °C) solution and stirring was continued at room temperature for 4 h. The solvent was removed, and the residue was dissolved in $CH_2Cl_2$(30 ml) and washed with $H_2O$ (3x20 ml). Removal of the dried solvent in vacuo gave a residue that was purified by flash chromatography eluting with $CH_2Cl_2$/MeOH/33% aq. $NH_4OH$ (9:1:0.05).

***tert*-butyl(4-((*tert*-butoxycarbonyl)(3-((*tert*-butoxycarbonyl)amino)propyl)amino)butyl)(3-((3-methoxybenzyl)amino)propyl)carbamate (24).** Synthesized from 3-methoxybenzaldehyde (0.151 g). Obtained 0.430 g of a yellow oil, 69 % yield. $^1$H-NMR (300 MHz, $CD_3Cl$) δ 1.45 (s, 27H), 1.63-1.76 (m, 6H), 2.64 (t, J = 6.6 Hz, 2H), 3.98-3.25 (m, 12H), 3.78 (s, 2H), 3.82 (s, 3H), 6.81 (d, J = 8.2 Hz, 1H), 6.92 (m, 2H), 7.25 (t, J = 7.2 Hz, 1H).

***tert*-butyl4-((*tert*-butoxycarbonyl)(3-((*tert*-butoxycarbonyl)amino)propyl)amino)butyl)(3-((4-methoxybenzyl)amino)propyl)carbamate (25).** Synthesized from 4-methoxybenzaldehyde (0.151 g). Obtained 0.450 g of a yellow oil, 72 % yield. $^1$H-NMR (300 MHz, $CD_3Cl$) δ 1.45 (s, 27H), 1.59-1.70 (m, 4H), 2.63-2.77 (m, 4H), 3.09-3.24 (m, 12H), 3.48 (s, 2H), 3.80 (s, 3h), 6.86 (d, J = 6.3 Hz, 2H), 7.27 (d, J = 6.6 Hz, 2H).

***tert*-butyl(4-((*tert*-butoxycarbonyl)(3-((*tert*-butoxycarbonyl)amino)propyl)amino)butyl)(3-((2-nitrobenzyl)amino)propyl)carbamate (26).** Synthesized from 2-nitrobenzaldehyde (0.166 g). Obtained 0.490 g of a yellow oil, 77 % yield. $^1$H-NMR (300 MHz, $CD_3Cl$)

δ 1.46 (s, 27H), 1.69-1.75 (m, 4H), 2.60-2.66 (m, 4H), 4.05 (s, 2H), 7.28-7.30 (m, 1H), 7.42-7.44 (m, 1H), 7.58-7.61 (m,1 H), 7.93-7.97d (m, 1H).

***tert*-butyl(4-((*tert*-butoxycarbonyl)(3-((*tert*-butoxycarbonyl)amino)propyl)amino)butyl)(3-((2-chlorobenzyl)amino)propyl)carbamate (27).** Synthesized from 2-chlorobenzaldehyde (0.154 g). Obtained 0.530 g of a yellow oil, 84 % yield. $^1$H-NMR (300 MHz, $CD_3Cl$) δ 1.45 (s, 27H), 1.63-1.75 (m, 6H), 2.64 (t, J = 6.6 Hz, 2H), 3.09-3.25 (m, 12H), 3.90 (s, 2H), 7.17-7.39 (m, 4H).

***tert*-butyl(4-((*tert*-butoxycarbonyl)(3-((*tert*-butoxycarbonyl)amino)propyl)amino)butyl)(3-((2,3,4-trimethoxybenzyl)amino)propyl)carbamate (28).** Synthesized from 2,3,4-trimethoxybenzaldehyde (0.216 g). Obtained 0.530 g of a yellow oil, 84 % yield. $^1$H-NMR (300 MHz, $CD_3Cl$) δ 1.39 (s, 27H), 1.60-1.67 (m, 6H), 2.56 (t, J = 6.2 Hz, 2H), 3.04-3.19 (m, 12H), 3.78 (s, 2H), 3.92 (s, 9H), 6.94-7.12 (m, 2H).

***tert*-butyl(4-((*tert*-butoxycarbonyl)(3-((*tert*-butoxycarbonyl)amino)propyl)amino)butyl)(3-((3,4,5-trimethoxybenzyl)amino)propyl)carbamate (29).** Synthesized from 3,4,5-trimethoxybenzaldehyde (0.216 g). Obtained 0.470 g of a yellow oil, 69 % yield. $^1$H-NMR (300 MHz, $CD_3Cl$) δ 1.44 (s, 27H), 1.63-1.76 (m, 6H), 2.64 (t, J = 6.2 Hz, 2H), 3.07-3.22 (m, 12H), 3.72 (s, 2H), 3.81 (s, 3H), 3.85 (s, 6H), 6.60 (s, 2H).

***tert*-butyl(4-((*tert*-butoxycarbonyl)(3-((*tert*-butoxycarbonyl)amino)propyl)amino)butyl)(3-((pyridin-2-ylmethyl)amino)propyl)carbamate (30).** Synthesized from 2-pyridylcarboxaldehyde (0.118 g). Obtained 0.570 g of a yellow oil, 96 % yield. $^1$H-NMR (300 MHz, $CD_3Cl$) δ 1.46 (s, 27H), 1.62-1.76 (m,6H), 2.65 (s, J = 6.2 Hz, 2H), 3.90 (s, 2H), 7.14-7.33 (m, 2H), 7.61-7.69 (td, J = 7.6, 1.8 Hz, 1H), 8.55 (d, J = 4.6 Hz, 1H).

***tert*-butyl(4-((*tert*-butoxycarbonyl)(3-((*tert*-butoxycarbonyl)amino)propyl)amino)butyl)(3-((pyridin-4-ylmethyl)amino)propyl)carbamate (31).** Synthesized from 4-pyridylcarboxaldehyde (0.118 g). Obtained 0.460 g of a yellow oil, 96 % yield. . $^1$H-NMR (300 MHz, $CD_3Cl$) δ 1.457(s, 27H), 1.65-1.72 (m, 4H), 1.91-2.03 (m, 2H), 2.15-2.18 (m, 2H), 3.01-3.12 (m, 10H), 3.16-3.21 (m, 2H), 4.59 (s, 2H), 7.99 (d, 2H, J = 5.1 Hz), 8.65 (d, 2H, J = 4.8 Hz).

***tert*-butyl(4-((*tert*-butoxycarbonyl)(3-((*tert*-butoxycarbonyl)amino)propyl)amino)butyl)(3-((2-(trifluoromethyl)benzyl)amino)propyl)carbamate (32).** Synthesized from 2-trifluoromethylaldehyde (0.191 g). Obtained 0.350 g of a yellow oil, 89 % yield. $^1$H-NMR (300

MHz, $CD_3Cl$) δ 1.45 (s, 27H), 1.47-1.73 (m, 4H), 2.64 (t, 2H, J = 6.0 Hz), 3.08-3.24 (m, 12H), 3.94 (s, 2H), 7.18-7.29 (m, 2H), 7.75-7.92 (m, 2H).

***tert*-butyl(4-((*tert*-butoxycarbonyl)(3-((*tert*-butoxycarbonyl)amino)propyl)amino)butyl)(3-((3-chlorobenzyl)amino)propyl)carbamate (33).** Synthesized from 2-trifluoromethylaldehyde (0.191 g). Obtained 0.300 g of a yellow oil, 83 % yield. $^1$H-NMR (300 MHz, $CD_3Cl$) δ 1.47 (s, 27H), 1.62-1.75 (m, 4H), 2.64 (t, 2H, J = 6.2 Hz), 3.09-3.25 (m, 12H), 3.90 (s, 2H), 7.17-7.42 (m, 4H).

**General procedure for the synthesis of the target compounds (1, 2, 5-10, 14 and 15).**

A solution of the appropriate compounds (0.5 mmol) in 30 ml of MeOH and 20 ml of aq. HCl 3 M (10 ml) was stirred overnight at room temperature. Following solvent removal, the residue was washed with $Et_2O$. The resulting solid was filtered and dried to afford the corresponding tetrahydrochloride salt as a white solid. All the compounds were obtained in quantitative yields.

***N*$^1$-(3-aminopropyl)-*N*$^4$-(3-((3-methoxybenzyl)amino)propyl)butane-1,4-diamine (1).** $^1$H-NMR (300 MHz, $D_2O$)0δ 1.88−1.62 (m, 4H), 2.91-2.97 (m, 12H), 3.72 (s, 3H), 3.92-4.00 (m, 2H), 6.91-6.94 (m, 3H), 7.26-7.31 (m, 1H); $^{13}$C-NMR (75 MHz, $D_2O$) δ 22.67. 22.72, 22.69, 36.50, 43.90, 44.48. 46.93, 51.02, 55.41, 115.08, 115.31, 122.29, 130.53, 1 31.18, 159.20; MS ($ES^+$) 323 $(M+H)^+$.0 0 MHz, $CD_3Cl$) δ 22.67, 22.72, 23.70, 36.51, 43.90, 44.,159.20. MS ($ESI^+$) 162 $(M+2H)^{2+}$.

***N*$^1$-(3-aminopropyl)-*N*$^4$-(3-((4-methoxybenzyl)amino)propyl)butane-1,4-diamine (2).** $^1$H-NMR (300 MHz, $D_2O$) δ 1.60-1.64 (m, 4H), 1.90-1.99 (m, 4H), 2.93-3.01 (m, 12H), 3.72 (s, 3H), 4.06 (s, 2H), 6.91-6.94 (m, 2H), 7.27-7.31 (m, 2H); $^{13}$C-NMR (75 MHz, $D_2O$) δ 25.20, 25.28, 26.27, 39.08, 46.16, 47.05, 49.50, 53.21, 57.95, 117.14, 125.50, 134.06, 162.31; MS ($ES^+$) 323 $(M+H)^+$.

***N*$^1$-(3-aminopropyl)-*N*$^4$-(3-((2-nitrobenzyl)amino)propyl)butane-1,4-diamine (5). ).** $^1$H-NMR (300 MHz, $D_2O$) δ 1.65-1.68 (m, 4H), 1.93-2.00 (m, 4H), 2.95-3.09 (m, 10H), 3.21-3.26 (m, 2H), 4.42 (s, 2H), 7.57-7.65 (m, 2H), 7.71-7.75 (m, 1H), 8.15-8.17 (m, 1H); MS ($ESI^+$) 169 $(M+2H)^{2+}$.

***N*$^1$-(3-aminopropyl)-*N*$^4$-(3-((2-chlorobenzyl)amino)propyl)butane-1,4-diamine (6).** $^1$H-NMR (300 MHz, $D_2O$) δ 2.09-2.13 (m, 4H), 2.42-2.50 (m, 4H), 3.42-3.51 (m, 10H), 3.57-3.61 (m, 2H), 4.77 (s, 2H), 7.76-7.82 (m, 2H), 7.87-7.90 (m, 2H); MS ($ESI^+$) 164 $(M+2H)^{2+}$.

***N*$^1$-(3-aminopropyl)-*N*$^4$-(3-((2,3,4-trimethoxybenzyl)amino)propyl)butane-1,4-diamine (7).** $^1$H-NMR (300 MHz, $D_2O$) δ 1.79-1.83 (m, 4H), 2.10-2.18 (m, 4H), 3.12-3.21 (m, 12H), 3.91 (s, 3H), 3.92 (s, 3H), 3.98 (s, 3H) 4.25 (s, 2H), 6.94 (d, 1H, J = 8.8 Hz), 7.20 (d, 1H, J = 8.8 Hz); $^{13}$C-NMR (75 MHz, $D_2O$) δ 22.46, 22.68, 23.67, 36.48, 43.64, 44.44, 44.47, 46.94, 56.02, 60.95, 61.38, 108.27, 116.38, 126.66, 140.97, 151.70, 154.67; MS (ESI$^+$) 192 $(M+2H)^{2+}$.

***N*$^1$-(3-aminopropyl)-*N*$^4$-(3-((3,4,5-trimethoxybenzyl)amino)propyl)butane-1,4-diamine (8).** $^1$H-NMR (300 MHz, $D_2O$) δ 1.79-1.83 (m, 4H), 2.12-2.19 (m, 4H), 3.12-3.22 (m, 12H), 3.83 (s, 3H), 3.91 (s, 6H), 4.24 (s, 2H), 6.89 (s, 2H); $^{13}$C-NMR (75 MHz, $D_2O$) δ 22.60, 22.68, 23.67, 36.48, 43.77, 44.43, 44.47, 46.93, 51.25, 56.15, 60.85, 107.42, 126.93, 137.45, 152.77; MS (ESI$^+$) 192 $(M+2H)^{2+}$.

***N*$^1$-(3-aminopropyl)-*N*$^4$-(3-((pyridin-2-ylmethyl)amino)propyl)butane-1,4-diamine (9).** $^1$H-NMR (300 MHz, $D_2O$) δ 1.76-1.80 (m, 4H), 2.04-2.12 (m, 2H), 2.16-2.24 (m, 2H), 3.07-3.21 (m, 10H), 3.33-3.36 (m, 2H), 4.66 (s, 2H), 7.98-8.01 (m, 1H), 8.07-8.09 (m,1H), 8.49-8.54 (m, 1H), 8.82-8.83 (m, 1H); $^{13}$C-NMR (75 MHz, $D_2O$) δ 22.58, 22.68, 23.66, 36.45, 44.29, 44.47, 44.97, 46.91, 46.96, 48.11, 127.26, 127.41, 144.54, 145.49, 145.73; MS (ESI$^+$) 147 $(M+2H)^{2+}$.

***N*$^1$-(3-aminopropyl)-*N*$^4$-(3-((pyridin-4-ylmethyl)amino)propyl)butane-1,4-diamine (10).** $^1$H-NMR (300 MHz, $D_2O$) δ 1.64-1.68 (m, 4H), 1.94-2.00 (m, 2H), 2.06-2.11 (m, 2H), 2.95-3.09 (m, 10H), 3.20-3.24 (m, 2H), 4.52 (s, 2H), 8.05 (d, 2H, J = 5.1 Hz), 8.76 (d, 2H, J = 4.8 Hz), 8.49-8.54 (m, 1H), 8.82-8.83 (m, 1H); $^{13}$C-NMR (75 MHz, $D_2O$) δ 22.58, 22.69, 22.67, 36.49, 44.33, 44.48, 45.14, 46.98, 49.36, 127.34, 142.16, 150.96; MS (ESI$^+$) 147 $(M+2H)^{2+}$.

***N*$^1$-(3-aminopropyl)-*N*$^4$-(3-((2-(trifluoromethyl)benzyl)amino)propyl)butane-1,4-diamine (14).** $^1$H-NMR (300 MHz, $D_2O$) δ 1.64-1.68 (m, 4H), 1.93-2.09 (m, 4H), 2.76-3.06 (m, 10H), 3.16-3.18 (m, 2H), 4.34 (s, 2H), 7.51-7.55 (m, 2H), 7.56-7.64 (m, 1H), 7.72-7.74 (m, 1H); MS (ESI$^+$) 181 $(M+2H)^{2+}$.

***N*$^1$-(3-aminopropyl)-*N*$^4$-(3-((2-fluorobenzyl)amino)propyl)butane-1,4-diamine (15).** $^1$H-NMR (300 MHz, $D_2O$) δ 1.61-1.68 (m, 4H), 1.93-2.03 (m, 4H), 2.95-3.10 (m, 12H), 4.22 (s, 2H), 7.11-7.8 (m, 2H), 7.35-7.43 (m, 2H); MS (ESI$^+$) 156 $(M+2H)^{2+}$.

**General procedure for the synthesis of 15 and 16**

A solution of **13** or **14** (1 eq) and 2-methylbenzaldehyde (1 eq) in toluene (10 ml) was stirred at the refluxing temperature in a Dean-Stark apparatus for 3 h. After cooling, the solvent was evaporated, and the residue was dissolved in EtOH (10 ml), cooled in an ice bath, and treated with $NaBH_4$ (4 eq); the reaction mixture was stirred 4h at room temperature. The solvent was then removed and the residue was dissolved in DCM (20 ml) and washed with $H_2O$ (3 x 20 ml). Removal of the dried solvent in vacuo gave a residue that was purified by flash chromatography with a mixture of petroleum ether/$CH_2Cl_2$/MeOH/33% aq. $NH_4OH$ (5:4:1:0.02) to give **15** or **16** as a yellow oil.

**tert-butyl (8-((3-((2-methylbenzyl)amino)propyl)amino)octyl)carbamate (37):** compound **35** (0.200 g, 0.7 mmol), 2-methylbenzaldehyde (0.7 mmol, 0.090 g, 0.08 ml), sodium borohydride (2.8 mmol, 0.106 g); yield 64%. $^1$H-NMR (400 MHz, $CdCl_3$) δ 1.28 (s, 9H), 1.44-1.51 (m, 12H). 1.75-1.79 (m, 2H), 2.23 (s, 3H), 2.61-2.63 (m, 2H), 2.75-2.79 (m, 4H+2H exch $D_2O$), 3.08-3.10 (m, 2H), 3.77 (s, 2H), 4.67 (brs exch $D_2O$, 1H), 7.14-7.16 (m, 3H), 7.28-7.29 (m, 1H).

**tert-butyl (3-(4-(3-aminopropoxy)butoxy)propyl)carbamate (38):** compound **36** (0.213 g, 0.7 mmol), 2-methylbenzaldehyde (0.7 mmol, 0.090 g, 0.08 ml), sodium borohydride (2.8 mmol, 0.106 g); yield 54%. $^1$H-NMR (400 MHz, $CdCl_3$) δ 1.54 (s, 9H), 1.60-1.88 (m, 9H+2H exch $D_2O$), 2.36 (s, 3H), 2.75-2.81 (m, 2H), 3.17-3.27 (m, 2H), 3.42-3.54 (m, 8H), 3.77 (s, 2H), 5.03 (brs exch $D_2O$, 2H), 7.15-7.23 (m, 3H), 7.28-7.32 (m, 1H).

**General procedure for the synthesis of 19 and 21.** A solution of **37** or **38** in MeOH (10 ml) and HCl 3M (10 ml) was stirred overnight at room temperature. Following solvent removal, the residue was washed with Et2O (5 x20 ml). The resulting solid was filtered and dried to afford EB20 or EB22 as trihydrochloride salt.

**$N^1$-(3-((2-methylbenzyl)amino)propyl)octane-1,8-diamine 19.** White solid; quantitative yield; mp > 250 C; $^1$H-NMR (400 MHz, $D_2O$) δ 1.14-1.25 (m, 8H), 1.50-1-56 (m, 4H), 1.97-2.03 (m, 2h), 2.26 (s, 3H), 2.82-2.93 (m, 4H), 2.98-3-02 (m, 2H), 3.09-3.15 (m, 2H), 4.18 (s, 2H), 7.17-7.29 (m, 4H); $^{13}$C-NMR (100 MHz, $D_2O$) δ 18.29, 21.75, 22.58, 25.37, 25.47, 26.52, 27.81, 36.01, 36.94, 39.45, 44.26, 47.80, 48.50, 126.62, 128.93, 129.84, 130.15, 131.00, 137.71; MS (ESI+) m/z = 153 $(M + 2H)^{2+}$.

**3-(4-(3-aminopropoxy)butoxy)-N-(2-methylbenzyl)propan-1-amine 21.** White solid; quantitative yield; mp > 250 C; $^1$H-NMR (400 MHz, $D_2O$) δ 1.35-1.41 (m, 4H), 1.75-1.87 /m, 4H),

2.23 (s, 3H), 2.90-2.94 (m, 2H), 3.04-3.08 (m, 2H), 3.27-3.44 (m, 8H), 4.12 (s, 2H), 7.16-7.25 (m, 4H); $^{13}$C-NMR (100 MHz, $D_2O$) δ 18.38, 25.14, 26.43, 37.41, 45.40, 47.99, 67.45, 67.69, 70.28, 70.34, 126.53, 129.03, 129.62, 129.96, 130.88, 137.43; MS (ESI+) m/z = 309 $(M + H)^+$.

**Amine oxidase activity assay and kinetic analyses**

Bovine serum amine oxidase activity was determined by measuring hydrogen peroxide generation rate (one of the reaction products) by a peroxidase-coupled continuous assay previously described.[59] The $H_2O_2$ produced during Spm derivatives oxidation was continuously monitored by the change of absorbance at 555 nm, under continuous stirring, using an extinction coefficient, ε, of $2.2 \times 10^4$ $M^{-1}cm^{-1}$. Polyamine substrate concentration was varied in the range 0.5-100 μM.

All experiments were carried out in air-saturated solutions of 10 mM potassium phosphate buffer pH 7.6, at temperature 37°C ± 0.5°C. The specific activity of the BSAO preparations was 0.36±0.02 U/mg, where one enzyme unit is the amount of enzyme that transforms 1 μmol of benzylamine (standard substrate) per minute.[59] Protein concentration was measured according to the Bradford method,[60] which uses bovine serum albumin as a standard.

Steady state kinetic parameters ($V_{max}$ and $K_M$) were calculated by fitting the Michaelis-Menten equation to the experimental data (initial rate of reactions *vs* substrate concentrations), with Sigma Plot software, version 10.0 (Jandel Scientific, San Rafael, CA, USA) .

Catalytic constant ($k_c$) and catalytic efficiency ($k_c/K_M$) were calculated from the $V_{max}$, assuming a BSAO molecular mass of 170 kDa.[45]

**Computational studies**

**Modeling of compounds**

Derivatives **1-23** and Spm were all modeled through the free for academic MolEdit molecular editor (https://www.molsoft.com/moledit.html) embedded in the www.3d-qsar.com Py-MolEdit web app.[61] Canonical SMILES structures were obtained with a simple python script using the openbabel APIs[62] (Supporting Information Table S16).

**BSAO structures preparations**

The BSAO structures available from PDB, 1TU5 and 2PNC, were processed through the www.3d-qsar.com Py-PDB web app. The structures were retrieved and cleaned up of all ions and molecules

not involved in the catalytic process. Together with the standard aminoacid residues the TPQ and the catalytic copper ion were retained. The cleaned structures were then added of the hydrogens considering a pH of 7.6 and subjected to a short energy minimization (100 iterations of steepest descent and 50 iterations of conjugated gradient) with the universal force field (UFF) force field[63] as implemented in the openbabel suites. The BSAO apoproteins and the CLO ligand we saved separately in a dataset container.

**Reversible Molecular Docking**

Through the Py-Docking web app available in www.3d-qsar.com two docking programs, Smina[48] and Plants,[49] were applied to the 1TU5 and 2PNC BSAO complexes considering all the implemented scoring functions (vina, vinardo and ad4 for Smina, and PLP, PLP95 and ChemPLP for Plants). Re-docking and cross-docking assessment experiments were run directly through the www.3d-qsar.com server. All derivatives **1-23** and Spm were then docked using the most appropriate program/scoring function combination (see results section in the main text) saving in a separate dataset container the lowest docked conformations for each derivative. The default settings were used for the dockings except by setting a cubic box extending 30 Å centered to the CLO center of mass. For Smina an exhaustiveness of 32 was set and the search_speed key to 1 for Plants.

**Covalent Molecular Docking**

A procedure as previously described was applied.[64] For the covalent docking procedure, for each derivative the TPQ-PA adduct was firstly prepared by means of a SMILES structure. To this the TPQ SMILES structure deprived of the oxygen in position 5 was added in turn of each PA SMILES structure. Then the TPQ-PA SMILES adduct was converted into a three-dimensional (3-D) structure with openbabel at pH 7.6. The 3-D structure was then merged in the BSAO replacing the original TPQ structure and converted into a flexible residue PDBQT file format through the openbabel file format conversion utility. Then a water molecule was prepared as a fake ligand to be reversibly docked. The version 1.2 of Vina program[54] was used to run the docking simulations. The simulation was run by setting a 50 Å cubic box centered to the copper atom, an exhaustiveness of 32, 100 docked conformations and leaving all the other settings to the defaults. The 100 docked conformations of the TPQ-PA adducts were then separated and reversibly rescored with the same scoring function to select the best docked conformation.[42]

Each of the separated covalently docked PA conformations was locally minimized with Smina (1000 iterations) and the lowest energy complex was saved into a new series of the **1-23** PAs and Spm by maintaining the TPQ without the oxygen in position 5 to avoid overlaps and also to mimic the TPQ-PA association/dissociation. A further 1000 iterations of local minimization was run on each of the PA after the constitution of the full TPQ structure.

Each step during the process was run with either vina or vinardo scoring functions. The whole process is depicted in Figure 3 and Figure 4 and also described in the results section of the main text.

**3-D QSAR modeling**

**LB models.** The **1-23** and Spm structures prepared as above described were subjected to conformational search with three methods (Balloon, openbabel and RDKit) as implemented in the Py-ConfSearch web app available from www.3d-qsar.com saving 100 conformations for each derivative and setting a minimum value of 2 for the RMSD to prune similar conformations. The conformational analysis was then subjected to automatic molecular alignments using the Shape and RDKit methods (Py-Align web app in www.3d-qsar.com) and using all the implemented scoring functions. 16 different templates molecules were used in either the lowest energy or the longest conformation. The templates were selected based on the lowest or highest values of activity ($pK_M$ or $p[k_{cat}/K_M]$), logP, MR, TPSA, HDB, HBA, number of rotatable bonds, highest MW and longest molecule.

The aligned conformations were automatically saved into datasets and 3-D QSAR models elaborated by the Py-CoMFA web app for each dataset using the defaults settings (C.3 probe atom, grid step of 2.0 Å, grid extension of 5 Å, minimum sigma of 2.0, Gasteiger charge model, dielectric constant of 8 and a cutoff energy value of 30 kcal/mol). The highest $q^2$ endowed models were then subjected to a variable pretreatment optimization (VPO) by randomly varying the settings. 3000 VPO models were picked up among millions of combinations. The model characterized by the highest $q^2$ values was ultimately optimized by a feature selection with a standard implementation of a SA algorithm[65] with an initial temperature of 10, a final temperature of 0.01 and a descending gradient of 0.9999.

The results of the model were graphically inspected with UCSF Chimera ver 1.16[66] with the downloaded dataset molecules and the associated maps (PLS Coeff × Average MIF values). The

optimal number of principal components (PCs) was determined by the SDEP decrement, selecting the PCs in which at least a 5% decrement was observed.

**Mixed LB-SB models.** The mixed LB_SB 3-D QSAR models were elaborated applying directly the Py-CoMFA web app on the reversibly/covalently docked conformations using the same procedure to define the LB models.

## COMBINE models

COMBINE-like[67] models were built through the Py-ComBinE web app available from www.3d-qsar.com. Differently from the original Wade's method here per residue interaction energies are calculated with the Autodock force field (ver 4.2) directly on the PA/BSAO complexes. Four types of interaction were calculated (STE, ELE, DRY and HB) and used by block scaling each interaction block.[68] Similarly, as for the 3-D QSAR models, a SA feature selection (initial temperature of 10, a final temperature of 0.01 and a descending gradient of 0.9999) was run to obtain the final models. The model was inspected through histogram plots of the AACs associated with each residue. The optimal number of PCs was determined by the SDEP decrement, selecting the PCs in which at least a 5% decrement was observed.

## Data and Software Availability

All computation for the 3-D QSAR and COMBINE model generation were run on the 3d-qsar.com portal (https://www.3d-qsar.com/) freely available to anyone for not profit usage, designed and maintained by the authors. All other used stand alone or command line software was free and publicly available: UCSF Chimera (https://www.cgl.ucsf.edu/chimera/download.html), anaconda was used as python environment (https://www.anaconda.com/products/distribution) with the free and open source available libraries (RDKit – https://www.rdkit.org/; OpenMM - https://openmm.org/; sci-kit learn - https://scikit-learn.org/stable/ and openbabel - http://openbabel.org/).

The used proteins structure data were available from PDB. All structures were computed starting from SMILES structures and are available in the Supporting Information Table S16 and as excel file.

**Supporting Information:** Additional experimental details, methods, figures and calculations.

**Author Contributions:** E.A., R.R., A.M., M.L.D.P. and G.C. conceived this study and coordinated the collaboration among the authors. E.A., R.R., A.M., V.T., L.A., E.P., R.F., P.F., T.T., and L.R. performed all the experiments. E.A., R.R., A.M., M.L.D.P. and G.C. optimized the protocols for the analyses and techniques performed by 3-D QSAR and docking. M.F., E.P., A.G. and P.F. discussed the project, focusing on the use of the more active molecules in future therapeutic applications. All authors wrote the manuscript and all authors have read and approved the final manuscript.

**Funding:** This study was funded by the generous support of "La Sapienza" University of Rome and Italian MIUR (Ministero dell'Istruzione, dell'Università e della Ricerca), Dipartimenti di Eccellenza-L. (232/2016), AIRC IG 25833, Istituto Pasteur-Fondazione Cenci-Bolognetti, AFM-Telethon grant #21025. E.A. would like to thank Wakunaga Pharmaceutical Co. Ltd. (Japan) for the scholarship given to T.T. for the support of the PhD research work.

**Informed Consent Statement:** Not applicable.

**Data Availability Statement:** Data availability statements were all added in the whole text and Supporting Information are also enclosed.

**Acknowledgments:** The authors would like to thank the 'International Polyamine Foundation-ETS-ONLUS'.

**Conflicts of Interest:** The authors declare no conflict of interest.

## References


1. Pegg, A. E., Mammalian polyamine metabolism and function. *IUBMB Life* **2009**, 61, 880-894.
2. Li, J.; Beuerman, R.; Verma, C. S., Mechanism of polyamine induced colistin resistance through electrostatic networks on bacterial outer membranes. *Biochim Biophys Acta Biomembr* **2020**, 1862, 183297.
3. Li, J.; Meng, Y.; Wu, X.; Sun, Y., Polyamines and related signaling pathways in cancer. *Cancer Cell Int* **2020**, 20, 539.
4. Coni, S.; Di Magno, L.; Serrao, S. M.; Kanamori, Y.; Agostinelli, E.; Canettieri, G., Polyamine Metabolism as a Therapeutic Target inHedgehog-Driven Basal Cell Carcinomaand Medulloblastoma. *Cells* **2019**, 8.
5. Nowotarski, S. L.; Woster, P. M.; Casero, R. A., Jr., Polyamines and cancer: implications for chemotherapy and chemoprevention. *Expert Rev Mol Med* **2013**, 15, e3.
6. Casero, R. A., Jr.; Woster, P. M., Recent advances in the development of polyamine analogues as antitumor agents. *J Med Chem* **2009**, 52, 4551-4573.
7. Amendola, R.; Cervelli, M.; Fratini, E.; Sallustio, D. E.; Tempera, G.; Ueshima, T.; Mariottini, P.; Agostinelli, E., Reactive oxygen species spermine metabolites generated from amine oxidases and radiation represent a therapeutic gain in cancer treatments. *Int J Oncol* **2013**, 43, 813-820.
8. Kanamori, Y.; Finotti, A.; Di Magno, L.; Canettieri, G.; Tahara, T.; Timeus, F.; Greco, A.; Tirassa, P.; Gasparello, J.; Fino, P.; Di Liegro, C. M.; Proia, P.; Schiera, G.; Di Liegro, I.; Gambari, R.; Agostinelli, E., Enzymatic Spermine Metabolites Induce Apoptosis Associated with Increase of p53, caspase-3 and miR-34a in Both Neuroblastoma Cells, SJNKP and the N-Myc-Amplified Form IMR5. *Cells* **2021**, 10.
9. Murray Stewart, T.; Dunston, T. T.; Woster, P. M.; Casero, R. A., Jr., Polyamine catabolism and oxidative damage. *J Biol Chem* **2018**, 293, 18736-18745.
10. Ohkubo, S.; Mancinelli, R.; Miglietta, S.; Cona, A.; Angelini, R.; Canettieri, G.; Spandidos, D. A.; Gaudio, E.; Agostinelli, E., Maize polyamine oxidase in the presence of spermine/spermidine induces the apoptosis of LoVo human colon adenocarcinoma cells. *Int J Oncol* **2019**, 54, 2080-2094.
11. Pegg, A. E., Toxicity of polyamines and their metabolic products. *Chem Res Toxicol* **2013**, 26, 1782-1800.
12. Gupta, N.; Verma, K.; Nalla, S.; Kulshreshtha, A.; Lall, R.; Prasad, S., Free Radicals as a Double-Edged Sword: The Cancer Preventive and Therapeutic Roles of Curcumin. *Molecules* **2020**, 25.
13. Djavaheri-Mergny, M.; Wietzerbin, J.; Besancon, F., 2-Methoxyestradiol induces apoptosis in Ewing sarcoma cells through mitochondrial hydrogen peroxide production. *Oncogene* **2003**, 22, 2558-2567.
14. Devereux, W.; Wang, Y.; Stewart, T. M.; Hacker, A.; Smith, R.; Frydman, B.; Valasinas, A. L.; Reddy, V. K.; Marton, L. J.; Ward, T. D.; Woster, P. M.; Casero, R. A., Induction of the PAOh1/SMO polyamine oxidase by polyamine analogues in human lung carcinoma cells. *Cancer Chemother Pharmacol* **2003**, 52, 383-390.
15. Agostinelli, E.; Condello, M.; Tempera, G.; Macone, A.; Bozzuto, G.; Ohkubo, S.; Calcabrini, A.; Arancia, G.; Molinari, A., The combined treatment with chloroquine and the enzymatic oxidation products of spermine overcomes multidrug resistance of melanoma M14 ADR2 cells: a new therapeutic approach. *Int J Oncol* **2014**, 45, 1109-1122.
16. Agostinelli, E.; Vianello, F.; Magliulo, G.; Thomas, T.; Thomas, T. J., Nanoparticle strategies for cancer therapeutics: Nucleic acids, polyamines, bovine serum amine oxidase and iron oxide nanoparticles (Review). *Int J Oncol* **2015**, 46, 5-16.

17. Averill-Bates, D. A.; Cherif, A.; Agostinelli, E.; Tanel, A.; Fortier, G., Anti-tumoral effect of native and immobilized bovine serum amine oxidase in a mouse melanoma model. *Biochem Pharmacol* **2005**, 69, 1693-1704.
18. Calcabrini, A.; Arancia, G.; Marra, M.; Crateri, P.; Befani, O.; Martone, A.; Agostinelli, E., Enzymatic oxidation products of spermine induce greater cytotoxic effects on human multidrug-resistant colon carcinoma cells (LoVo) than on their wild-type counterparts. *Int J Cancer* **2002**, 99, 43-52.
19. Venditti, I.; Hassanein, T. F.; Fratoddi, I.; Fontana, L.; Battocchio, C.; Rinaldi, F.; Carafa, M.; Marianecci, C.; Diociaiuti, M.; Agostinelli, E.; Cametti, C.; Russo, M. V., Bioconjugation of gold-polymer core-shell nanoparticles with bovine serum amine oxidase for biomedical applications. *Colloids Surf B Biointerfaces* **2015**, 134, 314-321.
20. Wang, K. L., J.; Yi, Y.; Lv, B.; Wu, Y.; Wang, C.; Li, H.; Li, Y.; Liu, Y.; Cai, X.; Meng, X.; Jiang, X.; Zheng, X.; Zhou, Z.; Bu, W, Polyamine-activated carbonyl stress strategy for oxidative damage therapy. *Nano Today* **2022**, 42.
21. Holt, A.; Smith, D. J.; Cendron, L.; Zanotti, G.; Rigo, A.; Di Paolo, M. L., Multiple binding sites for substrates and modulators of semicarbazide-sensitive amine oxidases: kinetic consequences. *Mol Pharmacol* **2008**, 73, 525-538.
22. Lunelli, M.; Di Paolo, M. L.; Biadene, M.; Calderone, V.; Battistutta, R.; Scarpa, M.; Rigo, A.; Zanotti, G., Crystal structure of amine oxidase from bovine serum. *J Mol Biol* **2005**, 346, 991-1004.
23. Di Paolo, M. L.; Pesce, C.; Lunelli, M.; Scarpa, M.; Rigo, A., N-alkanamines as substrates to probe the hydrophobic region of bovine serum amine oxidase active site: a kinetic and spectroscopic study. *Arch Biochem Biophys* **2007**, 465, 50-60.
24. Di Paolo, M. L.; Stevanato, R.; Corazza, A.; Vianello, F.; Lunelli, L.; Scarpa, M.; Rigo, A., Electrostatic compared with hydrophobic interactions between bovine serum amine oxidase and its substrates. *Biochem J* **2003**, 371, 549-556.
25. Hartmann, C.; Klinman, J. P., Structure-function studies of substrate oxidation by bovine serum amine oxidase: relationship to cofactor structure and mechanism. *Biochemistry* **1991**, 30, 4605-4611.
26. Stevanato, R.; Mondovi, B.; Befani, O.; Scarpa, M.; Rigo, A., Electrostatic control of oxidative deamination catalysed by bovine serum amine oxidase. *Biochem J* **1994**, 299 ( Pt 1), 317-320.
27. Ragno, R.; Ballante, F.; Pirolli, A.; Wickersham, R. B., 3rd; Patsilinakos, A.; Hesse, S.; Perspicace, E.; Kirsch, G., Vascular endothelial growth factor receptor-2 (VEGFR-2) inhibitors: development and validation of predictive 3-D QSAR models through extensive ligand- and structure-based approaches. *J Comput Aided Mol Des* **2015**, 29, 757-776.
28. Ragno, R., www.3d-qsar.com: a web portal that brings 3-D QSAR to all electronic devices-the Py-CoMFA web application as tool to build models from pre-aligned datasets. *J Comput Aided Mol Des* **2019**, 33, 855-864.
29. Ballante, F.; Musmuca, I.; Marshall, G. R.; Ragno, R., Comprehensive model of wild-type and mutant HIV-1 reverse transciptases. *J Comput Aided Mol Des* **2012**, 26, 907-919.
30. Sabatino, M.; Rotili, D.; Patsilinakos, A.; Forgione, M.; Tomaselli, D.; Alby, F.; Arimondo, P. B.; Mai, A.; Ragno, R., Disruptor of telomeric silencing 1-like (DOT1L): disclosing a new class of non-nucleoside inhibitors by means of ligand-based and structure-based approaches. *J Comput Aided Mol Des* **2018**, 32, 435-458.
31. Silvestri, L.; Ballante, F.; Mai, A.; Marshall, G. R.; Ragno, R., Histone deacetylase inhibitors: structure-based modeling and isoform-selectivity prediction. *J Chem Inf Model* **2012**, 52, 2215-2235.
32. Emanuela, B.; Minarini, A.; Tumiatti, V.; Milelli, A.; Lunelli, M.; Pegoraro, M.; Rizzoli, V.; Di Paolo, M. L., Synthetic polyamines as potential amine oxidase inhibitors: a preliminary study. *Amino Acids* **2012**, 42, 913-928.

33. Rosini, M.; Budriesi, R.; Bixel, M. G.; Bolognesi, M. L.; Chiarini, A.; Hucho, F.; Krogsgaard-Larsen, P.; Mellor, I. R.; Minarini, A.; Tumiatti, V.; Usherwood, P. N.; Melchiorre, C., Design, synthesis, and biological evaluation of symmetrically and unsymmetrically substituted methoctramine-related polyamines as muscular nicotinic receptor noncompetitive antagonists. *J Med Chem* **1999**, 42, 5212-5223.
34. Minarini, A.; Milelli, A.; Tumiatti, V.; Rosini, M.; Lenzi, M.; Ferruzzi, L.; Turrini, E.; Hrelia, P.; Sestili, P.; Calcabrini, C.; Fimognari, C., Exploiting RNA as a new biomolecular target for synthetic polyamines. *Gene* **2013**, 524, 232-240.
35. Bonaiuto, E.; Milelli, A.; Cozza, G.; Tumiatti, V.; Marchetti, C.; Agostinelli, E.; Fimognari, C.; Hrelia, P.; Minarini, A.; Di Paolo, M. L., Novel polyamine analogues: from substrates towards potential inhibitors of monoamine oxidases. *Eur J Med Chem* **2013**, 70, 88-101.
36. Wellendorph, P.; Jaroszewski, J. W.; Hansen, S. H.; Franzyk, H., A sequential high-yielding large-scale solution-method for synthesis of philanthotoxin analogues. *Eur J Med Chem* **2003**, 38, 117-122.
37. Hu, T.; Sun, D.; Zhang, J.; Xue, R.; Janssen, H. L. A.; Tang, W.; Dong, L., Spermine oxidase is upregulated and promotes tumor growth in hepatocellular carcinoma. *Hepatol Res* **2018**, 48, 967-977.
38. Kim, S.; Kim, D.; Roh, S.; Hong, I.; Kim, H.; Ahn, T. S.; Kang, D. H.; Lee, M. S.; Baek, M. J.; Kwak, H. J.; Kim, C. J.; Jeong, D., Expression of Spermine Oxidase Is Associated with Colorectal Carcinogenesis and Prognosis of Patients. *Biomedicines* **2022**, 10.
39. Di Paolo, M. L.; Cervelli, M.; Mariottini, P.; Leonetti, A.; Polticelli, F.; Rosini, M.; Milelli, A.; Basagni, F.; Venerando, R.; Agostinelli, E.; Minarini, A., Exploring the activity of polyamine analogues on polyamine and spermine oxidase: methoctramine, a potent and selective inhibitor of polyamine oxidase. *J Enzyme Inhib Med Chem* **2019**, 34, 740-752.
40. Bernstein, F. C.; Koetzle, T. F.; Williams, G. J.; Meyer, E. F., Jr.; Brice, M. D.; Rodgers, J. R.; Kennard, O.; Shimanouchi, T.; Tasumi, M., The Protein Data Bank: a computer-based archival file for macromolecular structures. *J Mol Biol* **1977**, 112, 535-542.
41. Caroli, A.; Ballante, F.; Wickersham, R. B., 3rd; Corelli, F.; Ragno, R., Hsp90 inhibitors, part 2: combining ligand-based and structure-based approaches for virtual screening application. *J Chem Inf Model* **2014**, 54, 970-977.
42. Ragno, R.; Frasca, S.; Manetti, F.; Brizzi, A.; Massa, S., HIV-reverse transcriptase inhibition: inclusion of ligand-induced fit by cross-docking studies. *J Med Chem* **2005**, 48, 200-212.
43. Dove, J. E.; Schwartz, B.; Williams, N. K.; Klinman, J. P., Investigation of spectroscopic intermediates during copper-binding and TPQ formation in wild-type and active-site mutants of a copper-containing amine oxidase from yeast. *Biochemistry* **2000**, 39, 3690-3698.
44. Janes, S. M.; Mu, D.; Wemmer, D.; Smith, A. J.; Kaur, S.; Maltby, D.; Burlingame, A. L.; Klinman, J. P., A new redox cofactor in eukaryotic enzymes: 6-hydroxydopa at the active site of bovine serum amine oxidase. *Science* **1990**, 248, 981-987.
45. Bellelli, A.; Morpurgo, L.; Mondovi, B.; Agostinelli, E., The oxidation and reduction reactions of bovine serum amine oxidase. A kinetic study. *Eur J Biochem* **2000**, 267, 3264-3269.
46. Dawkes, H. C.; Phillips, S. E., Copper amine oxidase: cunning cofactor and controversial copper. *Curr Opin Struct Biol* **2001**, 11, 666-673.
47. Ballante, F.; Ragno, R., 3-D QSAutogrid/R: an alternative procedure to build 3-D QSAR models. Methodologies and applications. *J Chem Inf Model* **2012**, 52, 1674-1685.
48. Quiroga, R.; Villarreal, M. A., Vinardo: A Scoring Function Based on Autodock Vina Improves Scoring, Docking, and Virtual Screening. *PLoS One* **2016**, 11, e0155183.
49. Korb, O.; Stutzle, T.; Exner, T. E., Empirical scoring functions for advanced protein-ligand docking with PLANTS. *J Chem Inf Model* **2009**, 49, 84-96.
50. Kim, J.; Lee, I. N., Inactivation of bovine plasma amine oxidase by 1,1,1-trihalo-3-aminopropanes. *Bioorg Chem* **2017**, 75, 265-273.

51. Klema, V. J.; Wilmot, C. M., The role of protein crystallography in defining the mechanisms of biogenesis and catalysis in copper amine oxidase. *Int J Mol Sci* **2012**, 13, 5375-5405.
52. Elovaara, H.; Kidron, H.; Parkash, V.; Nymalm, Y.; Bligt, E.; Ollikka, P.; Smith, D. J.; Pihlavisto, M.; Salmi, M.; Jalkanen, S.; Salminen, T. A., Identification of two imidazole binding sites and key residues for substrate specificity in human primary amine oxidase AOC3. *Biochemistry* **2011**, 50, 5507-5520.
53. Jakobsson, E.; Nilsson, J.; Ogg, D.; Kleywegt, G. J., Structure of human semicarbazide-sensitive amine oxidase/vascular adhesion protein-1. *Acta Crystallogr D Biol Crystallogr* **2005**, 61, 1550-1562.
54. Eberhardt, J.; Santos-Martins, D.; Tillack, A. F.; Forli, S., AutoDock Vina 1.2.0: New Docking Methods, Expanded Force Field, and Python Bindings. *J Chem Inf Model* **2021**, 61, 3891-3898.
55. Vainio, M. J.; Johnson, M. S., Generating conformer ensembles using a multiobjective genetic algorithm. *J Chem Inf Model* **2007**, 47, 2462-2474.
56. Mladenovic, M.; Patsilinakos, A.; Pirolli, A.; Sabatino, M.; Ragno, R., Understanding the Molecular Determinant of Reversible Human Monoamine Oxidase B Inhibitors Containing 2H-Chromen-2-One Core: Structure-Based and Ligand-Based Derived Three-Dimensional Quantitative Structure-Activity Relationships Predictive Models. *J Chem Inf Model* **2017**, 57, 787-814.
57. Kurtanovic, N.; Tomasevic, N.; Matic, S.; Mitrovic, M. M.; Kostic, D. A.; Sabatino, M.; Antonini, L.; Ragno, R.; Mladenovic, M., Human estrogen receptor alpha antagonists, part 2: Synthesis driven by rational design, in vitro antiproliferative, and in vivo anticancer evaluation of innovative coumarin-related antiestrogens as breast cancer suppressants. *Eur J Med Chem* **2022**, 227, 113869.
58. Mihovic, N.; Tomasevic, N.; Matic, S.; Mitrovic, M. M.; Kostic, D. A.; Sabatino, M.; Antonini, L.; Ragno, R.; Mladenovic, M., Human Estrogen Receptor alpha Antagonists. Part 1: 3-D QSAR-Driven Rational Design of Innovative Coumarin-Related Antiestrogens as Breast Cancer Suppressants through Structure-Based and Ligand-Based Studies. *J Chem Inf Model* **2021**, 61, 5028-5053.
59. Stevanato, R.; Mondovi, B.; Sabatini, S.; Rigo, A., Spectrophotometric Assay for Total Polyamines by Immobilized Amine Oxidases. *Anal Chim Acta* **1990**, 237, 391-397.
60. Bradford, M. M., A rapid and sensitive method for the quantitation of microgram quantities of protein utilizing the principle of protein-dye binding. *Anal Biochem* **1976**, 72, 248-254.
61. Ragno, R.; Esposito, V.; Di Mario, M.; Masiello, S.; Viscovo, M.; Cramer, R. D., Teaching and Learning Computational Drug Design: Student Investigations of 3D Quantitative Structure-Activity Relationships through Web Applications. *J Chem Educ* **2020**, 97, 1922-1930.
62. O'Boyle, N. M.; Banck, M.; James, C. A.; Morley, C.; Vandermeersch, T.; Hutchison, G. R., Open Babel: An open chemical toolbox. *J Cheminform* **2011**, 3, 33.
63. Rappe, A. K.; Casewit, C. J.; Colwell, K. S.; Goddard, W. A.; Skiff, W. M., Uff, a Full Periodic-Table Force-Field for Molecular Mechanics and Molecular-Dynamics Simulations. *J Am Chem Soc* **1992**, 114, 10024-10035.
64. Ortar, G.; Morera, E.; De Petrocellis, L.; Ligresti, A.; Schiano Moriello, A.; Morera, L.; Nalli, M.; Ragno, R.; Pirolli, A.; Di Marzo, V., Biaryl tetrazolyl ureas as inhibitors of endocannabinoid metabolism: modulation at the N-portion and distal phenyl ring. *Eur J Med Chem* **2013**, 63, 118-132.
65. Kirkpatrick, S.; Gelatt, C. D., Jr.; Vecchi, M. P., Optimization by simulated annealing. *Science* **1983**, 220, 671-680.
66. Pettersen, E. F.; Goddard, T. D.; Huang, C. C.; Couch, G. S.; Greenblatt, D. M.; Meng, E. C.; Ferrin, T. E., UCSF Chimera--a visualization system for exploratory research and analysis. *J Comput Chem* **2004**, 25, 1605-1612.
67. Wang, T.; Wade, R. C., Comparative binding energy (COMBINE) analysis of OppA-peptide complexes to relate structure to binding thermodynamics. *J Med Chem* **2002**, 45, 4828-4837.

68. Cruciani, G.; Watson, K. A., Comparative molecular field analysis using GRID force-field and GOLPE variable selection methods in a study of inhibitors of glycogen phosphorylase b. *J Med Chem* **1994**, 37, 2589-2601.

# New BSAO Substrates

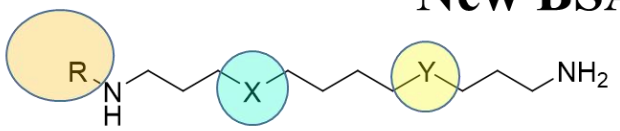


| # | R | X | Y | Km (μM) | $k_{cat}/K_m$ ($\mu M^{-1} s^{-1}$) |
|---|---|---|---|---|---|
| 10 | | N | N | 7.2 | 0.109 |
| 13 | | N | N | 6.0 | 0.098 |
| 21 | | O | O | 3.8 | 0.124 |

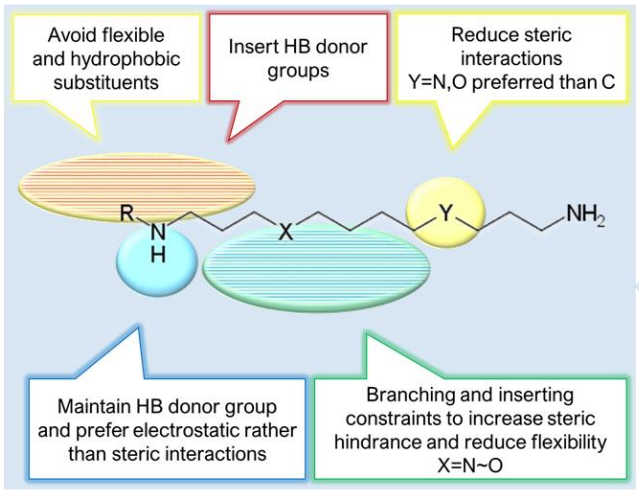


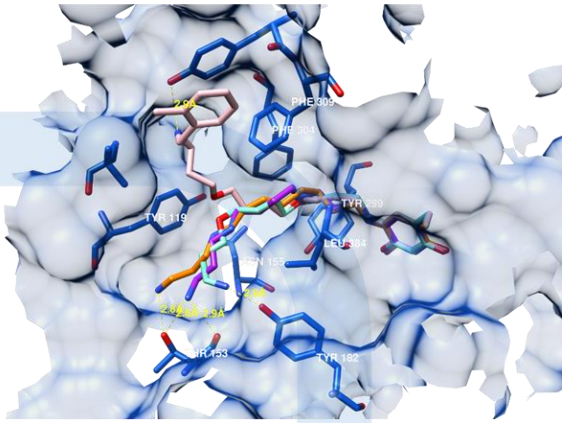

Molecular Docking

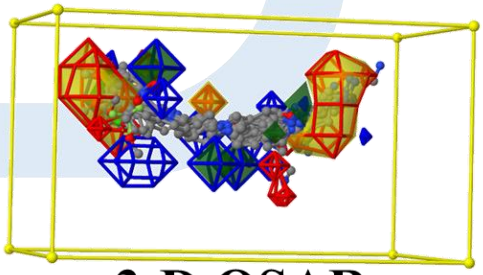

3-D QSAR